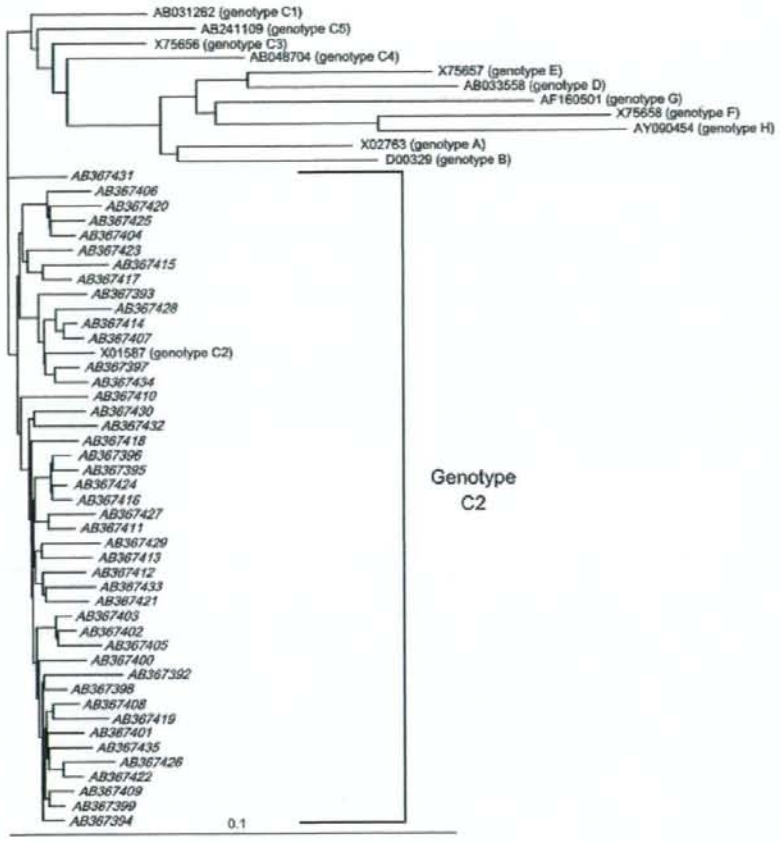

Figure 1. Phylogenetic tree analysis including 44 lamivudine-resistant hepatitis B virus (HBV) strains obtained in the present study and 12 representative HBV strains of various genotypes. All HBV strains are represented as GenBank accession nos., and the 44 lamivudine-resistant HBV strains are indicated by italics.

night incubation at 37°C in buffer containing 1% sodium dodecyl sulfate and 0.5 mg/mL proteinase K, followed by phenol/chloroform extraction and ethanol precipitation. The DNA sample was subjected to Southern blot analysis to detect HBV DNA, using a nonradioactive detection system (Alkphos Direct; GE Healthcare Life Sciences). Finally, the signals were analyzed quantitatively using image analyzing software (ImageJ; version 1.38). To detect extracellular HBV DNA, the transfection was scaled up to the 60-mm-diameter culture dish. After clarification by centrifugation at 8300 *g* for 30 min, the culture medium (3 mL) was centrifuged through a 20% sucrose cushion at 192,000 *g* for 4 h, using the Beckmann SW55Ti rotor. Then, DNA was extracted from the pellet and subjected to Southern blot analysis as described above. HBsAg and HBeAg in the culture medium were measured by chemiluminescent immunoassay.

Statistical analysis. Statistical analysis was performed by the χ^2 test, Fisher's exact test, and the Mann-Whitney *U* test. The results for the in vitro transfection study were examined by 1-way analysis of variance, and pairwise comparison was done by Fisher's protected least significant difference test. $P < .05$ was considered to indicate statistical significance.

RESULTS

Patient clinical characteristics and lamivudine resistance-associated mutations. All 44 HBV strains obtained from the patients with lamivudine-resistant CH-B comprised 3161–3230 nt in length and belonged to genotype C2, the most prevalent type in Japan (figure 1). As for lamivudine resistance-associated mutations in these strains, the rtM204V mutation was observed in 16 strains (36%), whereas the remaining 28 strains (64%) had the rtM204I mutation. The compensatory rtL180M mutation was found in 30 strains (68%). All 16 strains with rtM204V and 14 (50%) of the 28 strains with rtM204I possessed the rtL180M

Table 1. Clinical features of patients with lamivudine-resistant type B chronic hepatitis, according to the mutational status of rt180 and rt204.

Clinical feature	rt180 status			rt204 status		
	rtL180M positive (n = 30)	rtL180M negative (n = 14)	P	rtM204V (n = 16)	rtM204I (n = 28)	P
Age, years	48 (25–74)	55 (27–71)	NS	48 (25–74)	51 (27–71)	NS
Sex, M/F, no.	25/5	12/2	NS	13/3	24/4	NS
Liver disease, chronic hepatitis/cirrhosis/ hepatocellular carcinoma, no.	26/3/1	8/4/2	NS	13/2/1	21/5/2	NS
ALT level, IU/L	66 (11–331)	67 (25–393)	NS	85 (17–261)	54 (11–393)	NS
HBeAg, positive/negative, no.	23/7	8/6	NS	13/3	18/10	NS
HBV DNA level, $\log_{10}$ copies/mL	7.5 (3.5 to >7.6)	7.1 (3.6 to >7.6)	NS	7.5 (3.8 to >7.6)	7.1 (3.5 to >7.6)	NS
Previous IFN therapy, no. (%)	6 (20)	2 (14)	NS	3 (19)	5 (18)	NS
Combination therapy with IFN, no. (%)	10 (33)	6 (43)	NS	4 (25)	12 (43)	NS
Duration of lamivudine administration until point of analysis, years	2.9 (1.5–5.5)	2.2 (0.8–4.8)	NS	2.9 (1.5–5.5)	2.2 (0.8–4.8)	NS

NOTE. Data are median (range) values, unless otherwise indicated. HBeAg, hepatitis B e antigen; IFN, interferon; NS, not significant.

mutation, in agreement with previous reports with respect to the emergence pattern of the rtM204V/I and rtL180M mutations [15–17].

Various patient clinical characteristics were first correlated with the presence or absence of the rtL180M mutation or with the alternative of the rtM204V or rtM204I mutation in our 44 patients with CH-B (table 1). No differences were observed between patients with and those without the rtL180M mutation with respect to age, sex ratio, disease severity, ALT level, HBeAg positivity, serum HBV DNA level, frequency of previous IFN therapy, frequency of combination therapy with IFN, and total duration of lamivudine administration until the point of analysis. Also, there were no significant differences concerning these 9 characteristics between patients with virus having the rtM204V mutation and those with virus having the rtM204I mutation.

Genomic changes throughout the HBV genome associated with lamivudine resistance–associated mutations. Next, the genomic changes, which were significantly correlated with the occurrence of rtL180M or the preference for rtM204V or rtM204I, were investigated for the 44 HBV strains derived from the patients. As shown in table 2, 8 mutations and 1 deletion were identified as viral genomic changes significantly associated with the presence or absence of rtL180M. Among them, the A1896 mutation, which forms the in-frame stop codon in the

Table 2. Differences in the viral genome between lamivudine-resistant hepatitis B virus (HBV) strains with and those without the rtL180M mutation.

Viral genomic changes	Consensus nucleotide[a]	Amino acid substitution	rtL180M, no. (%)		P
			Positive (n = 30)	Negative (n = 14)	
Mutation					
A373	C	Pol-L428M (rtL82M)	0 (0)	3 (21)	<.05
T619	C	None	0 (0)	3 (21)	<.05
G739	T	Pol-M550V (rtM204V), surface-I95R	16 (53)	0 (0)	<.001
T/C/A741	G	Pol-M550I (rtM204I), surface-W96L/S/stop	14 (47)	14 (100)	<.001
A1896	G	Precore-W28stop	5 (17)	9 (64)	<.005
T2102	C	None	0 (0)	3 (21)	<.05
A/G2660	C	Pol-N118K	0 (0)	3 (21)	<.05
A2860	T	PreS1-S5T, pol-V184D[b]	0 (0)	4 (29)	<.01
Deletion					
6–54-bp deletion within nt 1–55	...	Truncation of 2–18 amino acids in preS2[c]	3 (10)	7 (50)	<.01

[a] Consensus nucleotides are derived from the genotype C2 HBV strain adr4 (GenBank accession no. X01587) [25].
[b] One patient had the pol-V184Q amino acid substitution due to a mutation in the adjacent nucleotide position.
[c] Detailed patterns of the preS2 deletion are shown in figure 2.

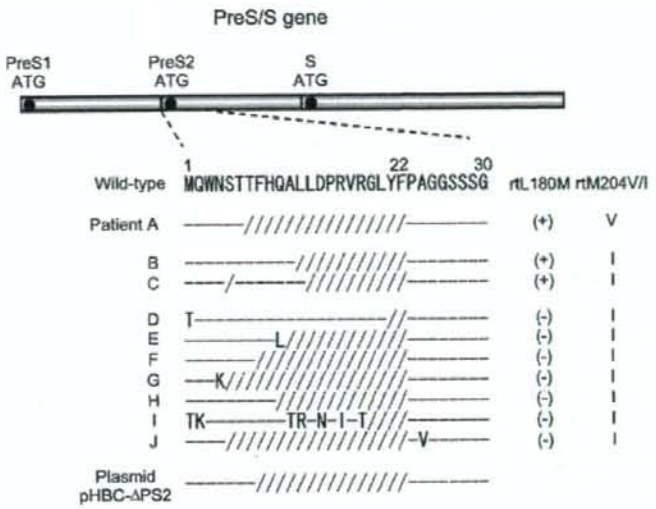

Figure 2. Patterns of the short deletion in the preS2 gene observed in lamivudine-resistant hepatitis B virus (HBV) strains. Ten of the 44 patients (patients A–J) had virus with the deletion in the preS2 gene of various patterns. The top sequence represents the amino acid sequence of the genotype C2 HBV DNA strain adr4 [25] as a representative strain. As for sequences derived from the patients, residues identical to the top sequence are indicated by dashes, whereas deletions of amino acid residues are shown by slashes. All deletions were found within the codon positions 5–22 of the preS2 gene. The bottom sequence represents the deletion pattern of the plasmid (pHBC-ΔPS2) used for in vitro transfection analysis (see figure 3), which expresses HBV DNA with the short deletion in the preS2 gene.

precore gene and results in the disability of HBeAg synthesis [26, 27], was found more frequently in viral strains without rtI80M than in those with it (64% vs. 17%; $P < .005$). Viral strains lacking rtL180M possessed the short deletion in the preS2 gene more frequently than those with rtL180M (50% vs. 10%; $P < .01$). The lengths of the deletion ranged from 12 to 54 bp, and all deletions were located within codon positions 5 to 22 of the preS2 gene (figure 2). Significant differences were also seen in the occurrences of 5 additional mutations—A373, T619, T2102, A/G2660, and A2860—between strains with and those without rtL180M. The detection rate of these 5 mutations was generally low among the lamivudine-resistant HBV strains obtained in this study. The G739 and T/C/A741 mutations are the causes of the rtM204V and rtM204I amino acid changes, and the occurrences of these mutations differed between viral strains with and those without rtL180M ($P < .001$), as described above.

Throughout the HBV genome, 5 mutations were significantly associated with the preference for the rtM204V or rtM204I mutation in the 44 lamivudine-resistant HBV strains (table 3). Of them, 3 mutations—C565, A853, and C1568—were found more frequently in strains with rtM204V than in those with rtM204I, but the frequencies of these mutations were considerably low in our lamivudine-resistant HBV strains. The occurrence of the A667 mutation, which accounts for rtL180M, was

Table 3. Differences in the viral genome between lamivudine-resistant hepatitis B virus (HBV) strains with the rtM204V and rtM204I mutations.

Mutation	Consensus nucleotide[a]	Amino acid substitution	No. (%) rtM204V ($n = 16$)	No. (%) rtM204I ($n = 28$)	P
C565	T	None	4 (25)	0 (0)	<.05
T/C646	A	Pol-V519L (rtV173L)	5 (31)	0 (0)	<.005
A667	T	Pol-L528M (rtL180M)	16 (100)	14 (50)	<.001
A853	C	None	3 (19)	0 (0)	<.05
C1568	T	Pol-L826P	3 (19)	0 (0)	<.05

[a] Consensus nucleotides are derived from the genotype C2 HBV strain adr4 (GenBank accession no. X01587) [25].

Table 4. Changing pattern of the precore defective A1896 mutation and short deletion in the preS2 gene from the pretreatment baseline to development of lamivudine resistance in relation to the presence or absence of the rtL180M mutation.

Type of mutation	Pattern of mutation		rtL180M, no.	
	Before therapy	After therapy*	Positive (n = 15)	Negative (n = 8)
Precore-defective A1896 mutation	−	−	8	2
	+	+	4	4
	−	+	1	2
	+	−	2	0
Short deletion in the preS2 gene	−	−	12	5
	+	+	0	1
	−	+	2	2
	+	−	1	0

* After development of lamivudine-resistant mutant virus.

higher in viral strains with rtM204V than in those with rtM204I ($P < .001$), as shown above. The T/C646 mutation, which causes the rtV173L change, was detected in 5 strains (31%) with rtM204V, compared with none of those with rtM204I ($P < .005$). It has been reported that the rtV173L mutation was detected together with the rtM204V and rtL180M mutations and was considered to be associated with lamivudine resistance [17, 28]. Our finding concerning the rtV173L mutation agreed with those of previous reports.

According to these observations, the relevance of the precore-defective A1896 mutation and the preS2 deletion to the absence of rtL180M was the most distinctive feature of the lamivudine-resistant HBV strains on screening of the whole genome. We therefore directed our attention to these precore and preS2 genomic changes and further investigated their role in the establishment of lamivudine-resistant virus.

Serial changes in the precore mutation and the preS2 deletion in lamivudine-resistant virus before and after lamivudine therapy. Serial changes in the precore-defective A1896 mutation, the short deletion in the *preS2* gene, and the drug resistance–associated rtM204V/I, rtL180M, and rtV173L mutations were investigated in the 23 (52%) of 44 patients with CH-B whose serum samples obtained before lamivudine therapy were available (table 4). Of the 11 patients with virus having the precore-defective mutation after the development of lamivudine resistance, 8 had virus that already possessed the mutation before therapy. Thus, the precore-defective mutation was generally a preexisting genomic change in most patients showing lamivudine resistance. On the other hand, of the 5 patients with virus that had the deletion in the preS2 gene after the development of drug resistance, 4 had virus that did not possess the deletion before therapy. The frequent detection of the preS2 deletion in lamivudine-resistant virus compared with virus before therapy indicates that this deletion may be coselected with drug resistance–associated mutations during the establishment of lamivudine-resistant mutant virus. As for the lamivudine-resistant rtM204V/I, rtL180M, and rtV173L mutations, they were not detected in any of the 23 viruses before lamivudine therapy, as expected.

Effect of the precore mutation and the preS2 deletion on the replicative competence of lamivudine-resistant HBV in vitro. We further conducted in vitro transfection analysis to explore the influence of the precore-defective mutation and the preS2 deletion on the replicative competence of lamivudine-resistant HBV. Three plasmids that expressed wild-type virus, precore-defective virus, and virus with the preS2 deletion were prepared. Next, plasmids with rtM204V plus L180M, rtM204I plus L180M, and rtM204I alone were synthesized in each of the 3 HBV-expressing backbone constructs. The level of intracellular HBV DNA was examined in cells transfected with these HBV-expressing plasmids. As shown in figure 3*A* and 3*B*, the introduction of lamivudine resistance–associated mutations into the virus with the wild-type backbone led to a decrease in viral replication (lanes 1–4). In addition, the replicative competence of the drug-resistant virus lacking rtL180M tended to be lower than that of the virus having rtL180M, although the difference was not statistically significant. As for the precore-defective virus, its replicative activity at baseline was higher than that of the wild-type virus (lanes 1 and 5). The decline in HBV replication due to the insertion of drug resistance–associated mutations was also observed for the virus with the precore-defective backbone. However, unlike for the virus with the wild-type backbone, the replicative activity of the precore-defective virus with lamivudine-resistant mutations was maintained at a considerable level (lanes 5–8). As for the virus with the preS2-deleted backbone, a reduction in viral replication due to the introduction of lamivudine resistance–associated mutations was also seen, but the degree of the reduction was not as great as that in the wild-type virus (lanes 9–12). Thus, both the precore-defective mutation and the preS2 deletion possessed activity supporting the viral replicative competence of lamivudine-resistant HBV, although the activity with the preS2 deletion was not as strong as that with the precore-defective mutation. The

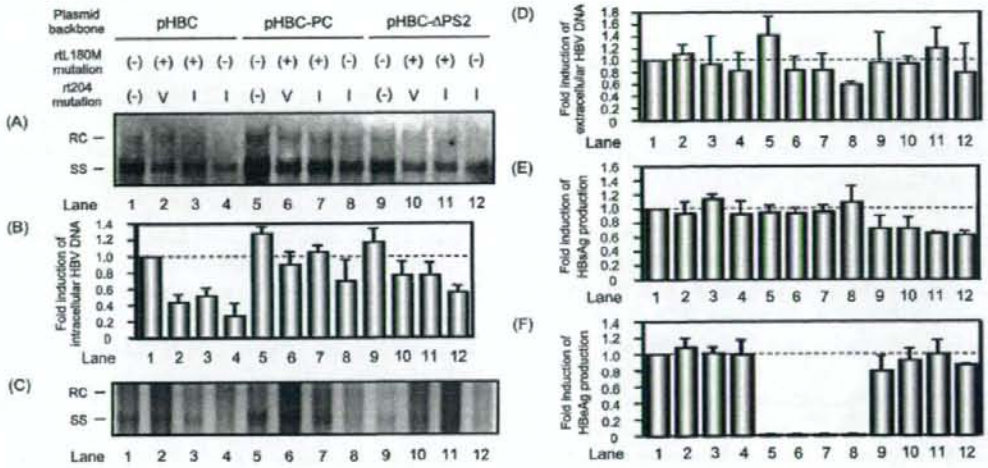

Figure 3. Levels of intracellular and extracellular progeny viral DNA and viral antigen production in cultured cells transfected with wild-type, precore-defective, or preS2-deleted hepatitis B virus (HBV)–expressing plasmids with or without lamivudine resistance-associated mutations. *A*, Representative result of Southern blot analysis to detect the intracellular progeny HBV DNA in cells transfected with various HBV-expressing plasmids. *B*, Quantitative analysis of the level of intracellular progeny HBV DNA. The progeny HBV DNA level for transfection with pHBC was considered to be 1, and the fold activities for transfection with the mutant HBV-expressing plasmids were calculated. The experiment was done 3 times, and results are shown as mean ± SD values. Statistically significant differences ($P < .05$) are as follows: lane 1 vs. 2–4, 1 vs. 5, 2 vs. 6 and 10, 3 vs. 7 and 11, 4 vs. 8 and 12, 5 vs. 6 and 8, and 9 vs. 10–12. *C*, Representative result of Southern blot analysis to detect extracellular progeny HBV DNA in cells transfected with various HBV-expressing plasmids. *D*, Quantitative analysis of the level of extracellular progeny HBV DNA. The progeny HBV DNA level for transfection with pHBC was considered to be 1, and the fold activities for transfection with the mutant HBV-expressing plasmids were calculated. The experiment was done 4 times, and results are shown as mean ± SD values. A statistically significant difference was not observed by 1-way analysis of variance. *E*, Levels of hepatitis B surface antigen (HBsAg) in culture medium of cells transfected with various HBV-expressing plasmids. The HBsAg level for transfection with pHBC was considered to be 1, and the fold activities for transfection with the mutant HBV-expressing plasmids were calculated. The experiment was done 3 times, and results are shown as mean ± SD values. Statistically significant differences ($P < .05$) are as follows: lanes 1 and 5 vs. 9, 3 and 7 vs. 11, and 4 and 8 vs. 12. *F*, Levels of hepatitis B e antigen (HBeAg) in culture medium of cells transfected with various HBV-expressing plasmids. The HBeAg level for transfection with pHBC was considered to be 1, and the fold activities for transfection with the mutant HBV-expressing plasmids were calculated. The experiment was done 3 times, and results are shown as mean ± SD values. Statistically significant differences ($P < .05$) are as follows: lanes 1 and 9 vs. 5, 2 and 10 vs. 6, 3 and 11 vs. 7, and 4 and 12 vs. 8. RC, relaxed circular HBV DNA; SS, single-stranded HBV DNA.

tendency appeared to be more evident in the drug-resistant virus without the rtL180M mutation. This may be a reason for the compensatory rtL180M mutation not being necessary during the establishment of lamivudine resistance in the HBV strain having the precore and preS2 genomic changes.

When the level of extracellular HBV DNA was examined in cells transfected with various HBV-expressing plasmids (figure 3*C* and 3*D*), no significant differences were observed among wild-type, precore-defective, and preS2-deleted viruses with respect to the reduction of viral secretion caused by the introduction of the lamivudine resistance–associated mutation. The discrepant results between the intracellular and extracellular viral DNA levels likely occurred because the extracellular viral DNA assay was less sensitive to minute changes in viral replication than the intracellular viral DNA assay.

As for the levels of production of HBsAg and HBeAg, the virus with the preS2-deleted backbone produced less HBsAg than did the viruses with the wild-type and precore-defective backbones (figure 3*E*). The wild-type and preS2-deleted viruses secreted HBeAg, whereas the precore-defective virus did not (figure 3*F*). The lamivudine resistance-associated mutations did not affect the production levels of HBV antigens.

DISCUSSION

HBV establishes lamivudine resistance via the resistance-causative rtM204V/I mutation and the replication-compensatory rtL180M mutation [15–20]. The present study aimed to investigate the genomewide peculiarity of lamivudine-resistant HBV. In particular, we elucidated the differences between viruses with and those without the compensatory rtL180M mutation. For this purpose, we conducted full-length sequencing analysis of lamivudine-resistant viruses derived from patients with CH-B by means of the PCR direct sequencing method. In some patients, the results were also confirmed by the PCR-subcloning method (data not shown). As a result, the precore-defective

A1896 mutation and the short deletion in the preS2 gene were identified as genomic changes significantly associated with the occurrence of the rtL180M mutation. These 2 viral genomic changes were found to be highly relevant to the observation that the rtL180M mutation was not needed for the establishment of the lamivudine-resistant mutant virus. This suggests that the precore-defective mutation and the preS2 deletion may function as surrogates for the compensatory rtL180M mutation and assist replication of lamivudine-resistant HBV. In the serial analysis of the mutations examined before and after lamivudine therapy, the preS2 deletion tended to be coselected with the drug resistance–associated mutation after therapy, although this tendency was not seen in the case of the precore-defective mutation. This also indicates that the preS2 deletion may have some advantage for establishment of lamivudine-resistant HBV.

We further conducted in vitro transfection analysis to verify the possible supportive role played by the precore and preS2 genomic changes in replication of lamivudine-resistant virus. The intracellular viral DNA was measured as a marker of viral replicative competence. In the wild-type virus, lamivudine resistance–associated mutations reduced viral replicative competence, and the rtL180M mutation compensated for viral replication to a certain degree. This agreed with previous findings of some other investigators [18–20]. On the other hand, the reduction in the viral replication level caused by the lamivudine-resistant mutations was lower in the precore-defective and preS2-deleted viruses than in the wild-type virus. Even the lamivudine-resistant virus without the rtL180M mutation maintained a substantial level of replicative activity in the viruses with precore and preS2 genomic changes. Thus, our results contribute evidence for a supportive role of both precore and preS2 genomic changes in the replicative competence of lamivudine-resistant HBV. This tendency was not evident in the case of the extracellular viral DNA assay, which may have been due to this assay's lower ability to detect slight changes in viral replicative activity.

As for the functional role played by the precore-defective A1896 mutation in the replication competence of lamivudine-resistant HBV, enhanced replicative activity of virus with lamivudine resistance caused by introduction of the precore-defective mutation has been reported for the recombinant HBV–expressing baculovirus system using the genotype D HBV strain [29]. Another previous in vitro transfection analysis using the genotype A HBV strain revealed that experimental insertion of the precore-defective mutation together with the T1858 mutation compensated for the replication competence of the virus possessing lamivudine-resistant mutations [30]. Our experimental result using the genotype C2 HBV strain is consistent with these previous findings. In addition, we showed in the present study that the preS2 deletion may also play a supportive role in the replication yield of lamivudine-resistant HBV, although the enhancement of viral replication caused by the preS2 deletion was not as strong as that caused by the precore-defective mutation.

It remains unclear why the precore-defective mutation leads to an increase in the viral replication of drug-resistant HBV. Previous in vitro transfection analyses have shown that the precore-defective mutation had no influence on viral replicative competence [29–31]. However, in our transfection analysis using the genotype C2 HBV strain, the replicative competence of the precore-defective virus tended to be higher than that of the wild-type virus, even when viruses without the lamivudine resistance–associated mutations were compared. It has recently been shown that the precore-defective mutation caused an elevation in viral replication in the particular HBV strain of genotype B1 [32]. According to this, the precore-defective mutation may in some way enhance HBV replication irrespective of the lamivudine resistance.

As for the involvement of the preS2 deletion in the replicative advantage of lamivudine-resistant HBV, the deletion results in truncation of the polymerase protein as well as the surface protein. Such truncation of the polymerase protein may increase the enzymatic activity and replication capacity of drug-resistant virus. As another possibility, the surface protein with the preS2 deletion may link to incomplete envelopment and subsequent intracellular accumulation of immature viral particles, resulting in an elevated intracellular HBV DNA level. However, this is improbable, because viral envelopment and secretion may be achieved efficiently in preS2-deleted virus as well as wild-type and precore-defective viruses, as was shown in the extracellular viral DNA assay.

In summary, our findings indicate that a precore-defective A1896 mutation and a short deletion in the preS2 gene may support viral replicative activity and substitute for the compensatory rtL180M mutation. Both the precore-defective mutation and the preS2 deletion have been shown to be frequently found during chronic HBV infection [26, 27, 33]. It is noteworthy that such naturally occurring frequent genomic changes in HBV significantly affect the establishment of drug-resistant viral strains. The lamivudine-resistant rtM204V/I mutation has also been reported to be completely or partially involved in resistance to other nucleos(t)ide analogues (emtricitabine, telbivudine, entecavir, and clevudine) [8, 9, 14, 34]. Our findings reveal novel aspects about the establishment of drug-resistant virus possessing the rtM204V/I and rtL180M mutations during the antiviral treatment of patients with CH-B.

References

1. Lai CL, Chien RN, Leung NW, et al. A one-year trial of lamivudine for chronic hepatitis B. Asia Hepatitis Lamivudine Study Group. N Engl J Med **1998**; 339:61–8.
2. Dienstag JL, Schiff ER, Wright TL, et al. Lamivudine as initial treatment for chronic hepatitis B in the United States. N Engl J Med **1999**; 341: 1256–63.

3. Hadziyannis SJ, Tassopoulos NC, Heathcote EJ, et al. Adefovir dipivoxil for the treatment of hepatitis B e antigen-negative chronic hepatitis B. Adefovir Dipivoxil 438 Study Group. N Engl J Med **2003**; 348:800–7.
4. Marcellin P, Chang TT, Lim SG, et al. Adefovir dipivoxil for the treatment of hepatitis B e antigen-positive chronic hepatitis B. Adefovir Dipivoxil 437 Study Group. N Engl J Med **2003**; 348:808–16.
5. Chang TT, Gish RG, de Man R, et al. A comparison of entecavir and lamivudine for HBeAg-positive chronic hepatitis B. BEHoLD AI463022 Study Group. N Engl J Med **2006**; 354:1001–10.
6. Lai CL, Shouval D, Lok AS, et al. Entecavir versus lamivudine for patients with HBeAg-negative chronic hepatitis B. BEHoLD AI463027 Study Group. N Engl J Med **2006**; 354:1011–20.
7. van Bommel F, Wunsche T, Mauss S, et al. Comparison of adefovir and tenofovir in the treatment of lamivudine-resistant hepatitis B virus infection. Hepatology **2004**; 40:1421–5.
8. Gish RG, Trinh H, Leung N, et al. Safety and antiviral activity of emtricitabine (FTC) for the treatment of chronic hepatitis B infection: a two-year study. J Hepatol **2005**; 43:60–6.
9. Lai CL, Leung N, Teo EK, et al. A 1-year trial of telbivudine, lamivudine, and the combination in patients with hepatitis B e antigen-positive chronic hepatitis B. Telbivudine Phase II Investigator Group. Gastroenterology **2005**; 129:528–36.
10. Marcellin P, Mommeja-Marin H, Sacks SL, et al. A phase II dose-escalating trial of clevudine in patients with chronic hepatitis B. Hepatology **2004**; 40:140–8.
11. Lai CL, Dienstag J, Schiff E, et al. Prevalence and clinical correlates of YMDD variants during lamivudine therapy for patients with chronic hepatitis B. Clin Infect Dis **2003**; 36:687–96.
12. Hadziyannis SJ, Tassopoulos NC, Heathcote EJ, et al. Long-term therapy with adefovir dipivoxil for HBeAg-negative chronic hepatitis B for up to 5 years. Adefovir Dipivoxil 438 Study Group. Gastroenterology **2006**; 131:1743–51.
13. Colonno RJ, Rose R, Baldick CJ, et al. Entecavir resistance is rare in nucleoside naive patients with hepatitis B. Hepatology **2006**; 44:1656–65.
14. Tenney DJ, Rose RE, Baldick CJ, et al. Two-year assessment of entecavir resistance in lamivudine-refractory hepatitis B virus patients reveals different clinical outcomes depending on the resistance substitutions present. Antimicrob Agents Chemother **2007**; 51:902–11.
15. Allen MI, Deslauriers M, Andrews CW, et al. Identification and characterization of mutations in hepatitis B virus resistant to lamivudine. Lamivudine Clinical Investigation Group. Hepatology **1998**; 27: 1670–7
16. Liaw YF, Chien RN, Yeh CT, Tsai SL, Chu CM. Acute exacerbation and hepatitis B virus clearance after emergence of YMDD motif mutation during lamivudine therapy. Hepatology **1999**; 30:567–72.
17. Westland CE, Yang H, Delaney WE 4th, et al. Activity of adefovir dipivoxil against all patterns of lamivudine-resistant hepatitis B viruses in patients. J Viral Hepat **2005**; 12:67–73.
18. Ono-Nita SK, Kato N, Shiratori Y, et al. Susceptibility of lamivudine-resistant hepatitis B virus to other reverse transcriptase inhibitors. J Clin Invest **1999**; 103:1635–40.
19. Melegari M, Scaglioni PP, Wands JR. Hepatitis B virus mutants associated with 3TC and famciclovir administration are replication defective. Hepatology **1998**; 27:628–33.
20. Ono SK, Kato N, Shiratori Y, et al. The polymerase L528M mutation cooperates with nucleotide binding-site mutations, increasing hepatitis B virus replication and drug resistance. J Clin Invest **2001**; 107:449–55.
21. Kobayashi S, Ide T, Sata M. Detection of YMDD motif mutations in some lamivudine-untreated asymptomatic hepatitis B virus carriers. J Hepatol **2001**; 34:584–6.
22. Kanada A, Takehara T, Ohkawa K, et al. Type B fulminant hepatitis is closely associated with a highly mutated hepatitis B virus strain. Intervirology **2007**; 50:394–401.
23. Kimura M. A simple method for estimating evolutionary rates of base substitutions through comparative studies of nucleotide sequences. J Mol Evol **1980**; 16:111–20.
24. Saitou N, Nei M. The neighbor-joining method: a new method for estimating and testing minimum-evolution trees. Mol Biol Evol **1987**; 4: 406–25.
25. Fujiyama A, Miyanohara A, Nozaki C, Yoneyama T, Ohtomo N, Matsubara K. Cloning and structural analyses of hepatitis B virus DNAs, subtype adr. Nucleic Acids Res **1983**; 11:4601–10.
26. Carman WF, Jacyna MR, Hadziyannis S, et al. Mutation preventing formation of hepatitis B e antigen in patients with chronic hepatitis B infection. Lancet **1989**; 2:588–91.
27. Okamoto H, Yotsumoto S, Akahane Y, et al. Hepatitis B viruses with precore region defects prevail in persistently infected hosts along with seroconversion to the antibody against e antigen. J Virol **1990**; 64:1298–303.
28. Delaney WE 4th, Yang H, Westland CE, et al. The hepatitis B virus polymerase mutation rtV173L is selected during lamivudine therapy and enhances viral replication in vitro. J Virol **2003**; 77:11833–41.
29. Chen RY, Edwards R, Shaw T, et al. Effect of the G1896A precore mutation on drug sensitivity and replication yield of lamivudine-resistant HBV in vitro. Hepatology **2003**; 37:27–35.
30. Tacke F, Gehrke C, Luedde T, Heim A, Manns MP, Trautwein C. Basal core promoter and precore mutations in the hepatitis B virus genome enhance replication efficacy of lamivudine-resistant mutants. J Virol **2004**; 78:8524–35.
31. Tong SP, Diot C, Gripon P, et al. In vitro replication competence of a cloned hepatitis B virus variant with a nonsense mutation in the distal pre-C region. Virology **1991**; 181:733–7.
32. Ozasa A, Tanaka Y, Orito E, et al. Influence of genotypes and precore mutations on fulminant or chronic outcome of acute hepatitis B virus infection. Hepatology **2006**; 44:326–34.
33. Sugauchi F, Ohno T, Orito E, et al. Influence of hepatitis B virus genotypes on the development of preS deletions and advanced liver disease. J Med Virol **2003**; 70:537–44.
34. Brunelle MN, Jacquard AC, Pichoud C, et al. Susceptibility to antivirals of a human HBV strain with mutations conferring resistance to both lamivudine and adefovir. Hepatology **2005**; 41:1391–8.

ELSEVIER

Journal of Hepatology 49 (2008) 779–786

Journal of Hepatology

www.elsevier.com/locate/jhep

Decreased expressions of CD1d molecule on liver dendritic cells in subcutaneous tumor bearing mice☆

Tomohide Tatsumi[1,2,3], Tetsuo Takehara[1,3], Shinjiro Yamaguchi[1,3], Akira Sasakawa[1,3], Masashi Yamamoto[1,3], Yui Fujita[1], Takuya Miyagi[1], Kazuyoshi Ohkawa[1], Norio Hayashi[1,3,*]

[1] *Department of Gastroenterology and Hepatology, Osaka University Graduate School of Medicine, 2-2 Yamadaoka, Suita, Osaka 565-0871, Japan*
[2] *Medical Center for Translational Research, Osaka University Hospital, Osaka 565-0871, Japan*
[3] *Core Research for Evolutional Science and Technology (CREST), Japan Science and Technology Agency (JST), Tokyo 150-0002, Japan*

***Background/Aims*: α-Galactosylceramide (α-GalCer) has been attracting attention as a novel approach to treat metastatic liver cancer. However, the activation of liver innate immunity by α-GalCer should be examined because clinical trials of α-GalCer resulted in limited clinical responses.**

***Methods*: We examined the activation of liver innate immunity by α-GalCer in subcutaneous Colon26 tumor bearing-mice (C26s.c.TB-mice).**

***Results*: The expressions of CD1d molecule on liver dendritic cells (DCs) were significantly lower in C26s.c.TB-mice than those in tumor-unbearing normal mice. Although liver NK cells and NKT cells activated in normal mice after α-GalCer treatment, the activation of these cells were significantly inhibited in C26s.c.TB-mice. α-GalCer treatment resulted in significant antitumor effect against Colon26 metastatic liver tumor in normal mice, but not in C26s.c.TB-mice. The serum levels of TGF-β, known to suppress the CD1d expressions on DCs, in C26s.c.TB-mice were significantly higher than those in normal mice. Surgical subcutaneous tumor mass reduction resulted in the reduction of serum TGF-β, the recovery of CD1d expressions on liver DCs and the improvement of antitumor effect of α-GalCer against metastatic liver tumor.**

***Conclusions*: These results suggested that tumor burden reduces CD1d expressions on liver DCs, thus impeding α-GalCer-mediated NK cell activation and antitumor activity in the liver.**

***Keywords*: α-Galactosylceramide; CD1d; Liver dendritic cells; Antitumor immunity**

1. Introduction

The glycolipid antigen α-galactosylceramide (α-GalCer) induces activation of NKT cells in a CD1d-dependent manner [1]. α-GalCer presented by DCs efficiently stimulates NKT cells implicated in the innate immunity [2,3]. Recently α-GalCer has been attracting attention for novel anti-tumor therapy. *In vivo* animal studies have shown that systemic administration of α-GalCer can lead to anti-tumor effects against metastatic liver tumor [4,5], suggesting that α-GalCer treatment might be promising for clinical application against liver tumor. Metastatic liver tumors, one of the most common types of advanced malignancy, resist conventional chemotherapy and radiotherapy, and present with a poor prognosis. Thus novel and more effective immunotherapy is needed, especially for metastatic liver cancer. Several phase I clinical studies have been carried

Received 29 February 2008; received in revised form 11 June 2008; accepted 14 June 2008; available online 2 July 2008
Associate Editor: V Barnaba

☆ The authors declare that they do not have anything to disclose regarding funding from industries or conflict of interest with respect to this manuscript.

* Corresponding author. Fax: +81 6 6879 3629.
E-mail address: hayashin@gh.med.osaka-u.ac.jp (N. Hayashi).

Abbreviations: DC, dendritic cell; APC, antigen-presenting cells; CTL, cytotoxic T lymphocytes; α-GalCer, α-galactosylceramide; M-NC, mononuclear cells; TB, tumor bearing.

0168-8278/$34.00 © 2008 Published by Elsevier B.V on behalf of the European Association for the Study of the Liver.
doi:10.1016/j.jhep.2008.06.011

out in cancer immunotherapy using intravenous administration of α-GalCer, but with limited clinical responses [6,7]. Most clinical trials of cancer immunotherapy have been conducted with patients at advanced stages of cancer. Thus, for further development of α-GalCer treatment in such patients, the antitumor effect of α-GalCer should be examined in hosts with an advanced tumor burden.

In the current study, we evaluated the anti-tumor effect of administration of α-GalCer against liver tumor in subcutaneous tumor bearing animals. Both the antitumor effect of α-GalCer against liver tumor and liver NK cell and NKT cells activation were impaired in subcutaneous tumor bearing mice (s.c.TB-mice). The liver DCs were poorly activated by α-GalCer administration with lower expression of CD1d, NKT-activating molecules. However, the CD1d expression increased and the antitumor effect of α-GalCer against liver tumor was improved after surgical resection of the subcutaneous tumor mass. Our study has shed light toward understanding of the antitumor effect of α-GalCer in metasatic liver cancer patients.

2. Materials and methods

2.1. Mice

Six-to-eight week old female BALB/c mice were purchased from Shizuoka Experimental Animal Laboratory (Shizuoka, Japan), and maintained in micro-isolator cages. The animals were handled under aseptic conditions. Procedures were performed according to approved protocols and in accordance with recommendations for the proper care and use of laboratory animals.

2.2. Cell lines

Colon26, a mouse colon adenocarcinoma cell line was kindly provided by Dr. Takashi Tsuruo (Institute of Molecular and Cellular Bioscience, The University of Tokyo, Tokyo, Japan). This cell line was maintained in complete medium (CM, RPMI-1640 medium supplemented with 10% heat-inactivated fetal bovine serum, 100 U/ml penicillin, 100 μg/ml streptomycin and 10 mM L-glutamine: all reagents from GIBCO/Life Technologies, Grand Island, New York) in a humidified incubator at 5% CO_2 and 37 °C.

2.3. α-GalCer

α-GalCer was kindly provided by Kirin Pharma Co. Ltd. (Gunma, Japan) and prepared as previously described [8].

2.4. Animal experiments

To establish Colon26 s.c.TB-mice (C26s.c.TB-mice), BALB/c mice were subcutaneously injected with 3×10^6 Colon26. On day 42, when the tumor size reached approximately 200 mm^2, bone marrow-derived DCs (BM-DCs) and liver DCs were prepared to evaluate the CD1d expression in C26s.c.TB-mice. BM-DC were generated as previously described [8]. Hepatic mononuclear cells (MNC) were prepared as previously described [8]. CD11c+ dendritic cells were isolated from hepatic MNC by magnetic cell sorting using MACS (Miltenyi Biotec, Gladbach, Germany) according to the manufacturer's protocol.

Hepatic metastasis of Colon26 cells was established as previously described [9]. To examine antitumor effect of α-GalCer in the liver of C26s.c.TB-mice, C26s.c.TB-mice or normal mice were injected with 5×10^5 Colon26 cells into the spleen 42 days after mice were subcutaneously injected with 3×10^6 Colon26 cells. Twenty-four hours later, α-GalCer (2 μg/100 μl) or 100 μl of the vehicle was administered intraperitoneally to each mouse. Ten days after tumor injection, the livers of the treated mice were removed, and the liver weight was measured to examine intrahepatic tumor growth.

2.5. Flow cytometry

For phenotypic analysis of BM-DCs and liver DCs, PE- or FITC-conjugated monoclonal antibodies (Ab) against mouse cell surface molecules [CD1d, CD80, CD86 CD11c (all from BD-Pharmingen, San Diego, CA), MHC class II (Miltenyi Biotec)], and appropriate isotype controls were used. We defined DCs with CD11c+ MHC class II+ cells by flow cytometry. To detect the NK cell and NKT cell population in liver MNCs, MNC were stained with PE-conjugated DX5 Ab and FITC-conjugated TCRβ (all from BD-Pharmingen). C26s.c.TB-mice and normal mice were injected intraperitoneally with α-GalCer (2 μg/100 μl) or 100 μl of vehicle. Hepatic MNC were prepared on day 0, 1, 3 and 7 after α-GalCer injection, and both NK cell and NKT cell populations in hepatic MNC were evaluated by flow cytometry. Flow cytometric analysis was performed using a FACscan (Becton Dickinson, San Jose, CA) flow cytometer. The results of flow cytometric analysis are reported in arbitrary mean fluorescence intensity (MFI) units.

2.6. TGF-β and IL-10 ELISA

Mice sera from C26s.c.TB-mice were harvested 42 days after intrahepatic tumor injection. Mice sera and the culture supernatants of Colon26 cells were subjected to mouse TGF-β ELISA (R&D systems, Minneapolis, MN) and mouse IL-10 ELISA (BD-Pharmingen), with lower levels of detection of 31.2 and 31.3 pg/ml, respectively.

2.7 Cytotoxic assay

To evaluate the activation of liver NK cells in C26s.c.TB-mice treated with α-GalCer, liver MNC were isolated 48 h after α-GalCer injection and subjected to ^{51}Cr release assay against NK-susceptible YAC-1 target as previously described [4]. Assays were performed in triplicate, with spontaneous release of all assays not exceeding 25% of the maximum release.

2.8. Surgical resection of subcutaneous tumor

To assess the impact of subcutaneous tumor on the CD1d expression of liver DCs, subcutaneous Colon26 tumors were surgically resected on day 42 after subcutaneous injection of Colon26 cells (C26s.c.TB-ope mice). Fourteen days after subcutaneous tumor resection, liver DCs were isolated and subjected to flow cytometry to evaluate the CD1d expression. To examine antitumor effect of α-GalCer in the liver of C26s.c.TB-ope mice, C26s.c.TB-mice or C26s.c.TB-ope mice were injected with 5×10^5 Colon26 cells into the spleen 10 days after subcutaneous tumor resection. Twenty-four hours later, α-GalCer (2 μg/100 μl) was administered intraperitoneally as above. Ten days later, the livers of the treated mice were removed, and the liver weights were measured to examine intrahepatic tumor growth.

2.9. Statistical analysis

The statistical significance of differences between the groups was determined by applying compared t test with Welch correction or Mann–Whitney U test. The statistical significance of the differences in more than three groups was determined by applying one-way ANOVA. We defined statistical significance as $p < 0.05$.

3. Results

3.1. Expressions of CD1d on DCs in C26s.c.TB-mice were lower than those in normal mice

Since α-GalCer induces activation of NKT cells in a CD1d-dependent manner [1], the expression of CD1d plays an important role in the activation of NKT cells. We examined the CD1d expressions on DCs in C26s.c.TB-mice. The expressions of CD1d on BM-DCs were similar in both normal and C26s.c.TB-mice (Fig. 1A and B). In contrast, those on liver DCs from C26s.c.TB-mice were significantly lower than those from normal mice (Fig. 1A and C). Spleen DCs from C26s.c.TB-mice were also significantly lower than those from normal mice (Fig. 1A and D). These results demonstrated that systemic decrease of CD1d expressions on DCs in each organ is observed in C26s.c.TB-mice, but the potential of differentiation of CD1d expressing DCs from precursor cells in bone marrow was similar between in C26s.c.TB-mice and normal mice.

3.2. The activation of liver NK cells, liver NKT cells and liver DCs was impaired in C26s.c.TB-mice

We next examined the activation of liver NK cells and liver NKT cells in C26s.c.TB-mice after administration of α-GalCer. The cytolytic activity of liver NK cells in α-GalCer-treated mice was stronger than that in vehicle-treated mice in normal mice. In marked contrast, the cytolytic activities in both α-GalCer and vehicle-treated mice were very weak in C26s.c.TB-mice (Fig. 2A). In normal mice, the liver NK cell proportions in whole liver MNCs increased with the peak at 1 day after α-

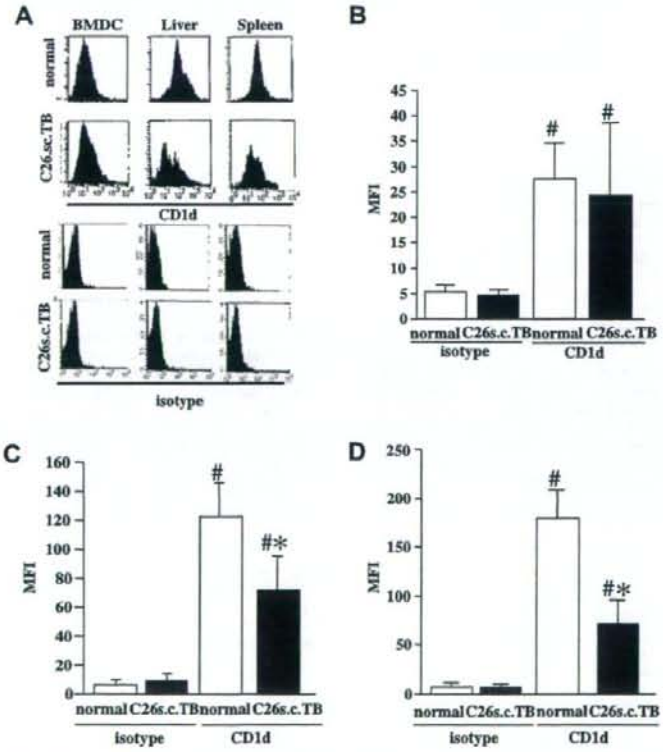

Fig. 1. CD1d expression on DCs in C26s.c.TB-mice. BM-DCs, liver and spleen DCs were prepared from C26s.c.TB-mice or normal mice ($N = 3$ in each group), and the expressions of CD1d molecules on DCs were evaluated by flow cytometry. The representative flow cytometry data of CD1d expressions on BM-DCs, liver DCs and spleen DCs were shown in Fig. 1A. The expression levels of CD1d molecules are reported in arbitrary MFI (mean ± SD). Normal: MFI of DCs from normal mice stained with anti-CD1d or isotype control antibody. C26s.c.TB: MFI of DCs from C26s.c.TB-mice stained with anti-CD1d or isotype control antibody. The CD1d expression on BM-DCs (B), on liver DCs (C), on spleen DCs (D). $^{\#}p < 0.05$ vs. respective isotype control $^{*}p < 0.05$ vs. CD1d expression in normal mice.

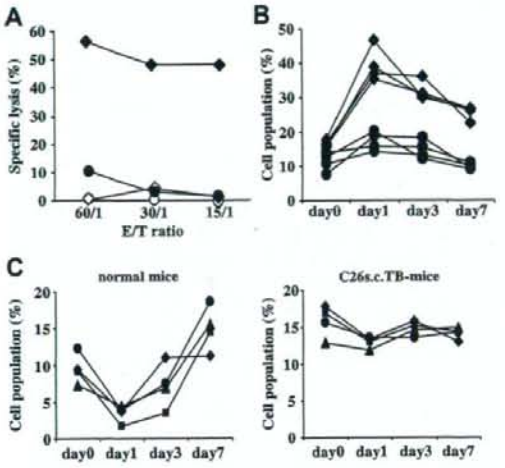

Fig. 2. Impaired activation of liver NK cells and NKT cells in C26s.c.TB-mice. (A) To evaluate the activation of liver NK cells in C26s.c.TB-mice treated by α-GalCer, liver MNC were isolated 48 h after α-GalCer injection and were subjected to ^{51}Cr release assay against NK-susceptible YAC-1 target. (♦) α-GalCer-treated normal mice, (◇) vehicle-treated normal mice, (•) α-GalCer-treated C26s.c.TB-mice, (○) vehicle-treated C26s.c.TB-mice. Representative data shown here is from three independent experiments. (B, C) BALB/c normal mice or C26s.c.TB-mice were injected intraperitoneally with α-GalCer. Hepatic MNC were prepared on day 0, 1, 3 and 7 days after α-GalCer injection. Liver NK cell and NKT cell populations in hepatic MNC were evaluated by flow cytometry. (B) Liver NK cell populations (DX5+/TCRβ− cells) in hepatic MNC after α-GalCer treatment. (♦) NK cell in each normal mice, (•) NK cell in each C26s.c.TB-mice ($N = 4$ in each group). (C) Liver NKT cell populations (DX5+/TCRβ+ cells) in hepatic MNC after α-GalCer treatment in normal mice and C26s.c.TB-mice ($N = 4$ in each group).

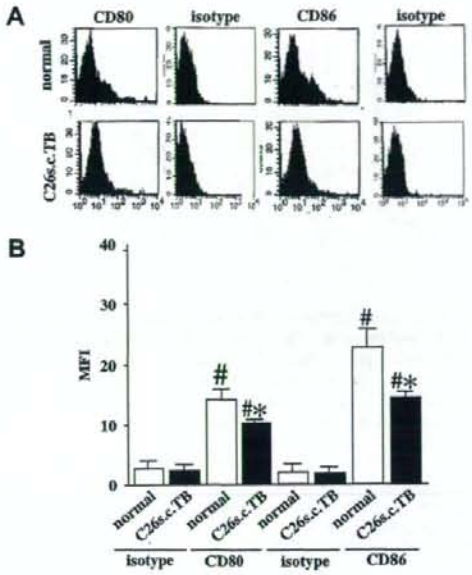

Fig. 3. The CD80 and CD86 expressions of liver DCs in C26s.c.TB-mice and normal mice. The expressions of CD80 and CD86 on liver DCs from both normal mice and C26s.c.TB-mice were evaluated by flow cytometry ($N = 3$ in each group). The representative flow cytometry data of CD80 and CD86 expressions on liver DC were shown in Fig. 3A. The expression levels of CD80 and CD86 molecules are reported as arbitrary MFI (mean ± SD of triplicate samples, Fig. 3B). $^{\#}p < 0.05$ vs. respective isotype control $^{*}p < 0.05$ vs. CD80 or CD86 expressions in normal mice.

GalCer administration, and the liver NK cell proportion at 7 days gradually decreased (Fig. 2B). C26s.c.TB-mice showed weaker increase of liver NK cell proportions in whole liver MNCs than normal mice (Fig. 2B). The liver NKT cell proportion decreased on day 1 and increased again on day 3 and day 7 after α-GalCer administration in normal mice. In marked contrast, those did not change on day 1, day 3 and day 7 after α-GalCer administration in C26s.c.TB-mice (Fig. 2C). The liver NK cell and NKT cell proportion in vehicle-treated mice exhibited no change in both mice groups (data not shown). These results demonstrated that the activation of liver NK cells and NKT cells by α-GalCer was impaired in C26s.c.TB-mice.

We also examined the CD80 and CD86 expressions of liver DCs in both C26s.c.TB-mice and normal mice, which are indicators of the antigen-presenting function of DCs. The expressions of CD80 and CD86 molecules on liver DCs from C26s.c.TB-mice were significantly lower than those from normal mice after α-GalCer administration (Fig. 3), suggesting that the antigen-presenting function of liver DC in C26s.c.TB-mice was also impaired compared with normal mice.

3.3. The antitumor effect of α-GalCer administration against metastatic liver tumor was impaired in C26s.c.TB-mice

We examined the antitumor effect of α-GalCer administration against metastatic liver tumor in both normal and C26s.c.TB-mice. With normal mice, no tumor formation was observed in the liver of any of the α-GalCer-treated mice although large Colon26 liver tumors had formed in all vehicle-treated mice. In contrast, with the C26s.c.TB-mice, large Colon26 liver tumors had formed in both α-GalCer-treated and vehicle-treated mice. The liver weights of the α-GalCer treatment group were significantly lighter than those of the vehicle treatment group for normal mice, while they were similar for both groups of the C26s.c.TB-mice (Fig. 4). These results demonstrated that the antitumor effect of α-GalCer against metastatic liver tumor was impaired in C26s.c.TB-mice.

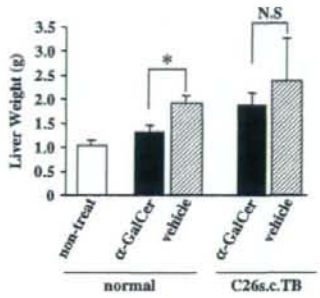

Fig. 4. Impaired antitumor effect of α-GalCer treatment against Colon26 liver tumor in C26s.c.TB-mice. To establish C26s.c.TB-mice, BALB/c mice were subcutaneously injected with 3×10^6 Colon26 cells 42 days before intrasplenic injection of tumor cells. BALB/c normal mice or C26s.c.TB-mice were injected into spleen with 5×10^5 Colon26 cells, and 24 h later either α-GalCer or vehicle was administered intraperitoneally ($N = 6$ in each treatment group). Ten days after treatment, the livers were removed from all treated mice and the liver weights of the groups were compared. As a control, the mean liver weights of untreated normal mice were 1.08 ± 0.09 g. $^*p < 0.05$. α-GalCer treatment group vs. vehicle treatment group in normal mice. N.S. α-GalCer treatment group vs. vehicle treatment group in C26s.c.TB-mice.

3.4. Serum TGF-β levels in C26s.c.TB-mice were increased compared with those in normal mice

Previous reports demonstrated that CD1d expressions on DCs decreased after co-culture with either TGF-β [10] or IL-10 [11]. The supernatants of 24 h cultures of Colon26 cells were subjected to TGF-β and IL-10 ELISA. The production of TGF-β in the supernatants of Colon26 was significantly higher than the control medium (Fig. 5A). No production of IL-10 was detected in the supernatants of Colon26 cells (data not shown). We next evaluate the serum TGF-β and IL-10 levels in C26s.c.TB-mice. The levels of TGF-β in C26s.c.TB-mice were significantly higher than that in normal mice (Fig. 5B). IL-10 was not detected in all mice sera from C26s.c.TB-mice and normal mice (data not shown).

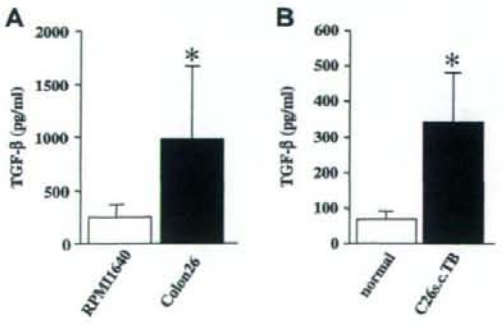

Fig. 5. The TGF-β production from Colon26 cells and the increase in serum TGF-β levels in C26s.c.TB-mice. (A) The culture supernatants of Colon26 cells or culture medium only (RPMI1640) were subjected to mouse TGF-β ELISA. (B) Mice sera from C26s.c.TB-mice were harvested 42 days after subcutaneous tumor injection and were subjected to mouse TGF-β ELISA. Mice sera from normal mice were used as controls. Cytokine levels are reported in pg/ml (mean ± SD of triplicate samples). Similar results were obtained in two independent experiments. $^*p < 0.05$.

3.5. Serum TGF-β levels decreased, the expression of CD1d molecules on liver DCs increased and the antitumor effect of α-GalCer was improved after tumor mass reduction

We next examined serum TGF-β levels and the CD1d expressions on liver DCs after surgical mass reduction in C26s.c.TB-mice. BALB/c mice were subcutaneously injected with 3×10^6 Colon26. On day 42, most Colon26 subcutaneous tumors were surgically excised (C26s.cTB-ope mice). Fourteen days later, serum TGF-β levels were evaluated, and liver DCs from C26s.c.TB-ope mice were prepared to evaluating the CD1d expression in comparison with those from C26s.c.TB-mice. The serum TGF-β levels in C26s.c.TB-ope mice were significantly lower than those in C26s.c.TB-mice (Fig. 6A). The expressions of CD1d on liver DCs from C26s.c.TB-ope mice were significantly higher than those from C26s.c.TB-mice and were similar to those from normal mice (Fig. 6B and C). These results demonstrated that surgical tumor mass reduction might lead to recovery of the impaired immune circumstances in the liver of C26s.c.TB-mice. We examined the antitumor effect of α-GalCer administration against metastatic liver tumor in both C26s.c.TB-mice and C26s.c.TB-ope mice. The liver weights of α-GalCer treated C26s.c.TB-ope mice were significantly lighter than those of α-GalCer treated C26s.c.TB-mice (Fig. 6D). These results demonstrated that the antitumor effect of α-GalCer against metastatic liver tumor was improved after subcutaneous tumor mass resection.

4. Discussion

A previous study showed that administration of α-GalCer resulted in complete rejection of Colon26 metastatic liver cancer in normal mice [5]. In the current study, we evaluated the antitumor effect of α-GalCer against the same Colon26 metastatic liver tumor model in C26s.c.TB-mice. α-GalCer treatment resulted in complete rejection of metasatic Colon26 liver tumor in normal mice, but the antitumor effect of α-GalCer against metastatic liver tumor was significantly impaired in C26s.c.TB-mice. These results were consistent with the clinical data of α-GalCer treatment in

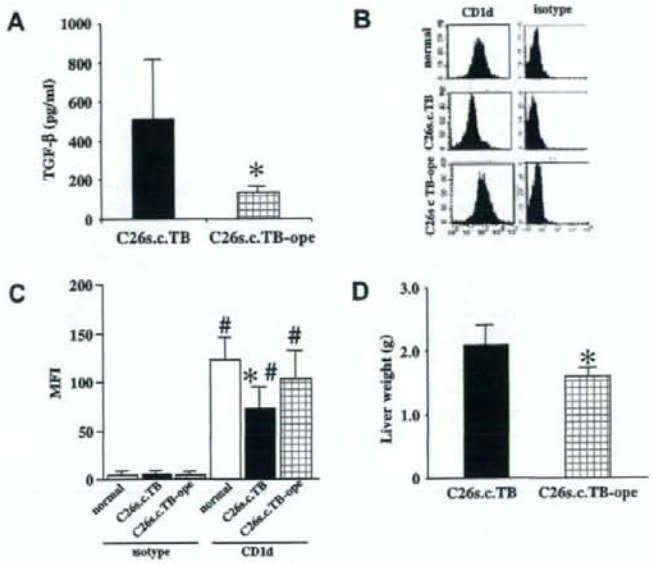

Fig. 6. Evaluation of serum TGF-β and CD1d expression on liver DCs and the antitumor effect of α-GalCer against metastatic liver tumor in surgical treated C26s.c.TB-mice. At 42 days, Colon26 subcutaneous tumors in C26s.c.TB-mice were surgically excised. Fourteen days later, liver DCs from surgically treated mice were prepared for comparison with liver DCs isolated from 42-day C26s.c.TB-mice. (A) Mice sera from C26s.c.TB-mice (C26s.c.TB) or surgically treated C26s.c.TB-mice (C26s.c.TB-ope) were harvested and were subjected to mouse TGF-β ELISA. Cytokine levels are reported in pg/ml (mean ± SD of triplicate samples). $^{*}p < 0.05$. (B, C) The expressions of CD1d on liver DCs from C26s.c.TB-mice (C26s.c.TB) or surgically treated C26s.c.TB-mice (C26s.c.TB-ope) were evaluated by flow cytometry. The representative flow cytometry data of CD1d expressions on liver DC were shown in Fig. 6B. The expression levels of CD1d molecules are reported as arbitrary MFI (mean ± SD of triplicate samples, Fig. 6C). $^{\#}p < 0.05$ vs. respective isotype control $^{*}p < 0.05$ vs. CD1d expression in normal mice. (D) C26s.c.TB-ope mice or C26s.c.TB-mice were injected into spleen with 5×10^5 Colon26 cells, and 24 h later α-GalCer was administered intraperitoneally ($N = 4$ in each group). Ten days after treatment, the livers were removed from treated mice and the liver weights of the groups were compared. $^{*}p < 0.05$. α-GalCer treated C26s.c.TB-ope mice vs α-GalCer treated C26s.c.TB-mice.

patients with advanced cancer, and encouraged us to investigate the detailed mechanism of the markedly reduced antitumor effect of α-GalCer in TB-mice to establish better α-GalCer treatment for cancer patients.

DCs have been implicated in the activation of NKT and NK cells in both mice and humans [1,6,12–17]. α-GalCer presented by CD1d molecules expressed on DCs activates NKT cells via recognition between CD1d molecules and Vα14–Jα281 invariant antigen receptor in mice [18]. Thus the expression of CD1d molecules on DCs is believed to be important for activation of NKT cells. Our study demonstrated that CD1d expressions on bone marrow-derived DCs were similar between normal and C26s.c.TB-mice, suggesting that the ability of differentiating DCs from precursor cells in bone marrow were same in both normal and C26s.c.TB-mice. In contrast, the CD1d expressions of liver DCs and spleen DCs in C26s.c.TB-mice were lower than those in normal mice. This is not unique to C26s.c.TB-mice, because decreased expression of CD1d molecules on liver DCs (not bone marrow-derived DCs) was also observed in CMS4 mouse sarcoma or BNL mouse hepatoma TB-mice (Tatsumi, unpublished data). These results suggested that some systemic immunosuppressive factors might modify the CD1d expression on DCs in TB-mice. Osman et al. demonstrated that α-GalCer administration resulted in activation of liver NKT cells with significant early disappearance of liver NKT cells in normal mice [19]. They also demonstrated that these phenomenon were not observed in CD1d(−/−) mice, suggesting that CD1d expressions play essential roles of liver NKT activation [19]. In our study, the early decreases of liver NKT cells were not observed after α-GalCer treatment in C26s.c.TB-mice. Based on these observations, the decreased expression of CD1d molecules on DCs might be associated with the impaired activation of liver innate immunity, thus resulting in an impaired antitumor effect of α-GalCer.

A normal mice liver contains lymphocytes that are usually enriched with NK and NKT cells; i.e., 25% NK cells and 30% NKT cells in contrast to peripheral blood that contains only 10% NK and 5% NKT cells

[20,21]. Efficient activation of abundant NKT cells and NK cells in the liver might be important in an antitumor effect against liver tumor. We and others have previously reported that sequential activation of both NKT cells and NK cells could be observed in the liver after α-GalCer administration. Although most NKT cells had disappeared from the liver within 12 h of α-GalCer administration [4,19], the antitumor effect against disseminated liver tumor depends on NK cells in the α-GalCer treatment, evidenced by that depletion of NK cells abolished the anti-metastatic tumor effect [4]. In the present study, we found the impairment of both the cytolytic activity of NK cells and an increase of the NK cell proportion in whole liver MNC in α-GalCer-treated C26s.c.TB-mice. These findings also offer the evidence that insufficient activation of liver NK cells might be associated with a poor antitumor effect of α-GalCer in TB-mice. The expressions of antigen-presenting related molecules, CD80 and CD86, on liver DCs in C26s.c.TB-mice were also lower than those in normal mice. Taken together, the presence of a tumor mass might modify the innate immune response in the liver and the maturation of liver DCs in TB-mice.

Several previous reports have demonstrated that TGF-β and IL-10 inhibit CD1d expression on DCs [10,11]. We hypothesize that the decreased expressions of CD1d might be associated with these immunosuppressive cytokines derived from the tumor mass. Our study demonstrated that Colon26 cells produce a large amount of TGF-β, but not IL-10, and that serum TGF-β level in C26s.c.TB-mice was significantly higher than that in normal mice, while the serum IL-10 level was not. Our results suggested that tumor-derived TGF-β might decrease CD1d expressions on liver DCs in C26s.c.TB-mice. Biswas et al. demonstrated that administration of anti-TGF-β neutralizing antibody inhibited metastatic cancer [22], suggesting that if the tumor-derived TGF-β had decreased in TB-mice, the liver immunological environment might be improved to develop antitumor immunity. Based on these results, we next examined serum TGF-β levels and the CD1d expression on liver DCs after surgical subcutaneous mass resection. Fourteen days after surgical resection, serum TGF-β in treated C26s.c.TB-mice had significantly decreased and the expressions of CD1d on liver DCs from treated C26s.c.TB-mice had significantly increased and recovered to the level of normal mice, suggesting that Colon26 tumor tissue derived TGF-β might modify the CD1d expression on liver DCs. More importantly, we demonstrated that the antitumor effect of α-GalCer against metastatic liver tumor was significantly improved in C26s.c.TB-ope mice. We believe that if complete resection of primary tumor could be achieved, the liver immune microenvironment might be expected to recover dramatically and cancer immunotherapy using α-GalCer might lead to better outcomes.

de Lalla et al. reported that the human invariant NKT cells are significantly enriched in chronically inflamed livers as compared with noninflamed ones although human liver harbors significantly less invariant NKT cells than the mouse one [23], suggesting that human invariant NKT cells might also play important roles in developing the chronic liver disease. Although the frequency of invariant Vα24 NKT cells is very low in humans, Vα24 NKT cells can be expanded by the stimulation of α-GalCer in cancer patients [7]. These suggested that the effector function of invariant NKT cells in human liver might be important for the establishing of new cancer treatments of α-GalCer.

The liver is the most common site of metastasis of gastrointestinal cancers (i.e., colorectal cancer, gastric cancer and pancreatic cancer). Thus, new therapeutic approaches of cancer immunotherapy for advanced liver tumor need to be developed. Our report is the first report demonstrating that the presence of a tumor mass might inhibit the activation of liver innate immune cells by α-GalCer due to decreased expression of CD1d on liver DCs. These findings indicate that α-GalCer treatment may represent a promising approach to preventing liver metastasis if the primary tumor can be completely controlled.

Acknowledgements

The authors thank Kirin Pharma Co. Ltd. (Gunma, Japan) for providing the α-galactosylceramide. This work was supported by a Grant-in-Aid from the Ministry of Education, Culture, Sports, Science and Technology of Japan, a Grant-in-Aid for Research on Hepatitis and BSE from the Ministry of Health, Labor and Welfare of Japan and Core Research for Evolutional Science and Technology (CREST) from Japan Science and Technology Agency.

References

[1] Kawano T, Cui J, Koezuka Y, Toura I, Kaneko Y, Sato H, et al. CD1d-restricted and TCR-mediated activation of Vα14NKT cells by glycosylceramides. Science 1997;278:1626–1629.
[2] Fujii S, Shimizu K, Kronenberg M, Steinman RM. Prolonged IFN-γ- producing NKT response induced with alpha-galactosylceramide-loaded DCs. Nat Immunol 2002;3:867–874.
[3] Gonzalez-Aseguinolaza G, de Oliveira C, Tomaska M, Hong S, Bruna-Romero O, Nakayama T, et al. α-Galactosylceramide-activated Vα 14 natural killer T cells mediate protection against murine malaria. Proc Natl Acad Sci USA 2000;97:8461–8466.
[4] Miyagi T, Takehara T, Tatsumi T, Kanto T, Suzuki T, Jinushi M, et al. CD1d-mediated stimulation of natural killer T cells selectively activates hepatic natural killer cells to eliminate experimentally disseminated hepatoma cells in murine liver. Int J Cancer 2003;106:81–89.
[5] Nakagawa R, Motoki K, Ueno H, Iijima R, Nakamura H, Kobayashi E, et al. Treatment of hepatic metastasis of the colon26

adenocacinoma with an α-galactosylceramide, KRN7000. Cancer Res 1998;58:1202–1207.
[6] Nieda M, Okai M, Tazbirkova A, Lin H, Yamaura A, Ide K, et al. Therapeutic activation of Vα24 + Vβ11 + NKT cells in human subjects results in highly coordinates secondary activation of acquired and innate immunity. Blood 2004;103:383–389.
[7] Giaccone G, Punt CJ, Ando Y, Ruijter R, Nishi N, Peters M, et al. A phase I study of the natural killer T-cell ligand α-galactosylceramide (KRN7000) in patients with solid tumors. Clin Cancer Res 2002;8:3702–3709.
[8] Tatsumi T, Takehara T, Yamaguchi S, Sasakawa A, Sakamori R, Ohkawa K, et al. Intrahepatic delivery of α-galatosylceramide pulsed dendritic cells suppresses liver tumor. Hepatology 2007;45:22–30.
[9] Takehara T, Uemura A, Tatsumi T, Suzuki T, Kimura R, Shiotani A, et al. Natural killer cell-mediated ablation of metastatic liver tumors by hydrodynamic injection of IFN alpha gene to mice. Int J Cancer 2007;120:1252–1260.
[10] Ronger-Savle S, Valladeau J, Claudy A, Schmitt D, Pequet-Navarro J, Dezutter-Dambuyant C, et al. TGFbeta inhibits CD1d expression on dendritic cells. J Invest Dermatol 2005;124:116–118.
[11] Gerlini G, Tun-Kyi A, Dudli C, Burg G, Pimpinelli N, Nestle FO. Metastatic melanoma secreted IL-10 down-regulates CD1 molecules on dendritic cells in metastatic tumor lesions. Am J Pathol 2004;165:1853–1863.
[12] Fernandez NC, Lozier A, Flament C, Ricciardi-Castagnoli P, Bellet D, Suter M, et al. Dendritic cells directly trigger NK cell functions: cross-talk relevant in innate anti-tumor immune responses in vivo. Nat Med 1999;5:405–411.
[13] Gerosa F, Baldani-Guerra B, Nisii C, Marchesini V, Carra G, Trinchieri G. Reciprocal activating interaction between natural killer cells and dendritic cells. J Exp Med 2002;195:327–333.
[14] Ferlazzo G, Tsang ML, Moretta L, Melioli G, Steinman RM, Munz C. Human dendritic cells activate resting NK cells and are recognized via the NKp30 receptor by activated NK cells. J Exp Med 2002;195:343–351.
[15] Kawano T, Cui J, Koezuka Y, Toura I, Kaneko Y, Sato H, et al. Natural killer-like nonspecific tumor cell lysis mediated by specific ligand-activated Vα14NKT cells. Proc Natl Acad Sci USA 1998;95:5690–5693.
[16] Kitamura H, Iwakabe K, Yahata T, Nishimura S, Ohta S, Ohmi Y, et al. The natural killer T (NKT) cell ligandα-galactosylceramide demonstrates its immunopoteniating effect by inducing interleukin (IL)-12 production by dendritic cells and IL-12 receptor expression on NKT cells. J Exp Med 1999;189:1121–1128.
[17] Ferlazzo G, Munz C. NK cell compartments and their activation by dendritic cells. J Immunol 2004;172:1333–1339.
[18] Seino K, Motohashi S, Fujisawa T, Nakayama T, Taniguchi M. Natural killer T cell-mediated antitumor immune responses and their clinical applications. Cancer Sci 2006;97:807–812.
[19] Osman Y, Kawamura T, Naito T, Takeda K, Van Kaer L, Okumura K, et al. Activation of hepatic NKT cells and subsequent liver injury following administration of α-galactosylceramide. Eur J Immunol 2000;30:1919–1928.
[20] Doherty DG, O'Farrelly C. Innate and adaptive lymphoid cells in human liver. Immunol Rev 2000;174:5–20.
[21] Mehal WZ, Azzaroli F, Crispe IN. Immunology of the healthy liver: old questions and new insights. Gatsroenterology 2001;120:250–260.
[22] Biswas S, Guix M, Rinehart C, Dugger TC, Chytil A, Moses HL, et al. Inhibition of TGF-beta with neutralizing antibodies prevents radiation-induced acceleration of metastatic cancer progression. J Clin Invest 2007;117:1305–1313.
[23] de Lalla C, Galli G, Aldrighhetti L, Romeo R, Mariani M, Monno A, et al. Production of profibrotic cytokines by invariant NKT cells characterizes cirrhosis progression in chronic viral hepatitis. J Immunol 2004;173:1417–1425.

JOURNAL OF VIROLOGY, Sept. 2008, p. 8349–8361 Vol. 82, No. 17
0022-538X/08/$08.00+0 doi:10.1128/JVI.00306-08

Intramembrane Processing by Signal Peptide Peptidase Regulates the Membrane Localization of Hepatitis C Virus Core Protein and Viral Propagation▽

Kiyoko Okamoto,[1]† Yoshio Mori,[1]† Yasumasa Komoda,[1] Toru Okamoto,[1] Masayasu Okochi,[2] Masatoshi Takeda,[2] Tetsuro Suzuki,[3] Kohji Moriishi,[1] and Yoshiharu Matsuura[1]*

Department of Molecular Virology, Research Institute for Microbial Diseases,[1] and Department of Post-Genomics and Diseases, Division of Psychiatry and Behavioral Proteomics, Graduate School of Medicine,[2] Osaka University, Osaka, and Department of Virology II, National Institute of Infectious Diseases, Tokyo,[3] Japan

Received 12 February 2008/Accepted 11 June 2008

Hepatitis C virus (HCV) core protein has shown to be localized in the detergent-resistant membrane (DRM), which is distinct from the classical raft fraction including caveolin, although the biological significance of the DRM localization of the core protein has not been determined. The HCV core protein is cleaved off from a precursor polyprotein at the lumen side of Ala[191] by signal peptidase and is then further processed by signal peptide peptidase (SPP) within the transmembrane region. In this study, we examined the role of SPP in the localization of the HCV core protein in the DRM and in viral propagation. The C terminus of the HCV core protein cleaved by SPP in 293T cells was identified as Phe[177] by mass spectrometry. Mutations introduced into two residues (Ile[176] and Phe[177]) upstream of the cleavage site of the core protein abrogated processing by SPP and localization in the DRM fraction. Expression of a dominant-negative SPP or treatment with an SPP inhibitor, L685,458, resulted in reductions in the levels of processed core protein localized in the DRM fraction. The production of HCV RNA in cells persistently infected with strain JFH-1 was impaired by treatment with the SPP inhibitor. Furthermore, mutant JFH-1 viruses bearing SPP-resistant mutations in the core protein failed to propagate in a permissive cell line. These results suggest that intramembrane processing of HCV core protein by SPP is required for the localization of the HCV core protein in the DRM and for viral propagation.

The hepatitis C virus (HCV), which has infected an estimated 170 million people worldwide, leads to chronic hepatitis, which in turn causes severe liver diseases, including steatosis, cirrhosis, and eventually hepatocellular carcinoma (47). HCV possesses a positive-sense single-stranded RNA with a nucleotide length of 9.6 kb, which encodes a single large precursor polyprotein composed of about 3,000 amino acids. The viral polyprotein is processed by cellular and viral proteases into structural and nonstructural proteins (24). The development of efficient therapies for hepatitis C had been hampered by the lack of a reliable cell culture system, as well as by the absence of a small-animal model. Lohmann et al. established an HCV replicon, which consisted of an antibiotic selection marker and a genotype 1b HCV RNA, and showed that it replicated autonomously in the intracellular compartments of a human hepatoma cell line, Huh7 (16). The replicon system has been used as an important tool in the investigation of HCV replication, and it has served as a cell-based assay system for the evaluation of antiviral compounds. Recently, cell culture systems for in vitro replication and infectious-virus production were established based on the full-length HCV genome of a genotype 2a isolate, which was recovered from a fulminant hepatitis C patient (15, 45, 50). However, the molecular mechanism of the HCV life cycle in host cells has not been well characterized.

Several viruses have been reported to utilize a lipid raft composed of cholesterol and sphingolipids upon entry (34). The lipid raft is characterized by resistance to nonionic detergents at 4°C and includes caveolin, glycolipids, and other substances (40). Several nonenveloped viruses enter cells through a caveola/raft-mediated endosome, designated the caveosome, and then translocate to the endoplasmic reticulum (ER), endosome, or nucleus (34, 35), although enveloped viruses generally enter host cells through a clathrin-dependent pathway (18). HCV is enclosed by a host cell-derived membrane and belongs to the family *Flaviviridae*. Several reports suggest that HCV enters host cells through general endocytosis, such as by a clathrin-mediated pathway (5, 6, 22). However, HCV has been suggested to replicate on a detergent-resistant membrane (DRM), including some characteristic membrane structures such as lipid rafts and membranous webs (8, 9, 38). In a previous report, an HCV replication complex prepared from a cell fraction treated with a nonionic detergent was shown to be enzymatically active (2). HCV nonstructural proteins remodel the intracellular membrane to form a replication complex that includes several host proteins (8, 46). The HCV core protein has a C-terminal transmembrane region that is anchored on intracellular compartments such as the ER and mitochondria and on the surfaces of lipid droplets (10, 30, 42). Recent studies have indicated that assembly of HCV particles occurs around lipid droplets that are surrounded by the remodeled membranes (23). Although the HCV core protein functions as a capsid protein, it is found in the DRM fraction, which is

* Corresponding author. Mailing address: Department of Molecular Virology, Research Institute for Microbial Diseases, Osaka University, 3-1 Yamada-oka, Suita, Osaka 565-0871, Japan. Phone: 81-6-6879-8340. Fax: 81-6-6879-8269. E-mail: matsuura@biken.osaka-u.ac.jp.
† K. Okamoto and Y. Mori contributed equally to this work.
▽ Published ahead of print on 18 June 2008.

distinct from the classical lipid rafts (20). However, the biological function of the HCV core protein localized in the DRM has not been clarified.

The HCV core protein is cleaved from a precursor polyprotein by a signal peptidase (SP) to liberate it from the envelope protein E1 and is then further processed by a signal peptide peptidase (SPP) (21). However, the biological significance of the intramembrane processing of the HCV core protein by SPP remains largely unknown. Furthermore, the C-terminal end of the mature HCV core protein expressed in insect cells has been reported to be Phe^{177} or Leu^{179} (12, 29), while that in mammalian cells has not been determined. Expression of SPP enhanced the accumulation of nonenveloped nucleocapsid and reduced that of enveloped nucleocapsid in yeast cells, suggesting that maturation of core protein is carried out after the formation of enveloped particles (17). However, the effect of SPP cleavage on viral assembly in mammalian cells has not been well characterized. Randall et al. have reported that introduction of a small interfering RNA targeted to SPP reduced the production of infectious HCV particles (36), suggesting that SPP is required for the production of HCV particles. In this study, we determined the cleavage site of the mature HCV core protein expressed in human cells and examined the biological significance of the intramembrane processing of the core protein by SPP for the localization of the core protein in the DRM and the production of infectious particles.

MATERIALS AND METHODS

Cell lines and HCV infection. HCV subgenomic RNA was removed from the replicon cell line 9-13 (16) by treatment with alpha interferon. A cell line that was highly permissive for JFH-1 infection was cloned from the resulting crude populations by the limited-dilution method and designated Huh7OK1 (32). The Huh7OK1 cell line retained the ability to produce type I interferons through the RIG-I-dependent signaling pathway upon infection with RNA viruses and exhibited a cell surface expression level of human CD81 comparable to that of the parental cell line. The detailed characteristics of this cell line will be described in a future communication. The HuhOK1 and Huh7.5.1 cell lines (the latter was kindly provided by F. Chisari) and the human embryonic kidney cell line 293T were maintained in Dulbecco's modified Eagle's medium supplemented with 10% fetal calf serum and nonessential amino acids (Sigma, St. Louis, MO). Huh7OK1 or Huh7.5.1 cells were infected with HCV strain JFH-1 as described by Wakita et al. (45). The plasmid carrying strain JFH-1 cDNA under the control of the pol1 promoter (19) was transfected into Huh7OK1 or Huh7.5.1 cells, and propagation of the JFH-1 virus was determined by the production of HCV core protein (as described below) and by the titration of infectious particles (39). The persistently infected Huh7OK1 cells were maintained under normal conditions after 8 passages before use. The 9-13 cell line, which possesses an HCV subgenomic replicon (16), was cultured in Dulbecco's modified Eagle's medium supplemented with 10% fetal calf serum and 1 mg/ml G418.

Plasmids. Genes encoding the N-terminally FLAG-tagged and/or C-terminally hemagglutinin (HA)-tagged core proteins derived from the HCV genotype 1b strain J1 or its mutants were introduced into plasmid vector pcDNA3.1 (Invitrogen, Carlsbad, CA) as described previously (30). Each insert gene was transferred into a pCAGGS vector (28) at the PmeI site. The resulting plasmids encoded the HCV core protein (amino acid residues 1 to 191) with or without FLAG and HA tags at the N and C termini, respectively. All of the core proteins with these tags (FLAG-core-HA proteins) had a mutation of Ala^{191} to Arg in order to prevent cleavage by the SP (7). Plasmid pHH21/JFH-1, carrying a full genomic cDNA of strain JFH-1 under the control of the pol1 promoter, was used to produce the infectious JFH-1 virus (19). An adaptive mutation of Leu to Val at amino acid position 758 in the p7 region was introduced during a long-term passage of the JFH-1 virus into Huh7.5.1 cells (data not shown). To improve the replication efficiency of the JFH-1 virus, a mutation of Leu to Val was introduced into pHH21/JFH-1 by site-directed mutagenesis, and the resulting plasmid was designated pHH21/JFH-1/L758V. To generate plasmids encoding the mutant JFH-1 viruses, the following substitutions were introduced into pHH21/JFH-1/L758V: Val^{139}, Val^{140}, and Leu^{144} were replaced with Ala (JFH-1/VVL/3A); $Ile^{176}$and Phe^{177} were replaced with Ala and Leu, respectively (JFH-1/IF/AL); Ala^{180}, Ser^{183}, and Cys^{184} were replaced with Val, Leu, and Val, respectively (JFH-1/ASC/VLV); and Asp^{2736} was replaced with Asn (JFH-1/GND).

Antibodies and reagents. Antisera against HCV genotype 1 or 2a core proteins were raised in rabbits by immunization with peptides corresponding to the region spanning residues 103 to 115, conserved among genotypes 1a and 1b, or to the region from residue 101 to 119 of genotype 2a (strain JFH-1). These peptides were synthesized and conjugated with keyhole limpet hemocyanin (Scrum Inc., Tokyo, Japan). Antisera were purified with an affinity column conjugated with the antigenic peptides. A monoclonal antibody to HCV NS5A (5A27) was prepared from BALB/c mice (CLEA Japan, Tokyo, Japan) immunized with the recombinant domain I of NS5A by a method described previously (31). Antibodies to caveolin-1, calreticulin, and the FLAG tag (M2) were purchased from Sigma. Antibodies to the HA tag and glyceraldehyde-3-phosphate dehydrogenase (GAPDH) were purchased from Babco (Richmond, CA) and Santa Cruz Biotechnology (Santa Cruz, CA), respectively. The aspartic protease inhibitors $(Z\text{-}LL)_2$ ketone and L685,458 were purchased from the Peptide Institute (Osaka, Japan). These inhibitors were dissolved in dimethyl sulfoxide and stored at −20°C until use.

Transfection, SDS-PAGE, and Western blotting. Huh7.5.1 and 293T cells were transfected with plasmids by lipofection with *Trans* IT LT-1 (Mirus, Madison, WI) and Lipofectamine 2000 (Invitrogen), respectively, according to the manufacturers' protocols. Cells were lysed on ice in Triton lysis buffer (20 mM Tris-HCl [pH 7.4], 135 mM NaCl, 1% Triton-X 100, 10% glycerol) supplemented with a protease inhibitor mix (Nacalai Tesque, Kyoto, Japan) at 24 or 48 h after transfection and were then subjected to sodium dodecyl sulfate-polyacrylamide gel electrophoresis (SDS-PAGE) using Tris-glycine buffer and Western blotting using appropriate antibodies as previously described (30). The stained protein bands were visualized using the SuperSignal West Femto enhanced-chemiluminescence substrate (Pierce, Rockford, IL) and an LAS3000 imaging system (Fuji Photo Film, Tokyo, Japan).

Determination of the expression of the C terminus of the mature HCV core protein in mammalian cells. Two million 293T cells cultured in a collagen-coated dish (diameter, 10 cm) were transfected with pCAGGS-FLAG-core (26) by lipofection, harvested at 20 h posttransfection with a rubber policeman after two washes with ice-cold phosphate-buffered saline (PBS), and collected by centrifugation at 1,000 × *g* for 5 min. The cells were lysed with 0.1 ml of triple-detergent lysis buffer (45 mM Tris-HCl [pH 7.4] containing 0.5% sodium deoxycholate, 0.1% SDS, 1% Triton X-100, 135 mM NaCl, and a protease inhibitor mix [Nacalai Tesque]) (24). The lysate was stored at −80°C until use. The lysate was thawed on ice and then centrifuged at 20,000 × *g* for 10 min at 4°C. The supernatant was mixed with 20 μl of 50% (vol/vol) anti-FLAG M2 affinity gel (Sigma) and then rotated at 4°C for 90 min. The gel beads were washed with the triple-detergent lysis buffer and then suspended in 30 μl of the loading buffer. The suspended gel beads were boiled for 5 min and then centrifuged at 20,000 × *g* for 5 min at room temperature. The resulting supernatant was subjected to SDS-PAGE, and the gel was stained with Sypro Ruby dye (Invitrogen). The portion of the gel including proteins with an expected molecular size of 20 kDa was excised from the stained gel, washed twice with 200 μl of 50 mM NH_4HCO_3 dissolved in 50% acetonitrile (vol/vol), and then immersed in 100 μl of 100% acetonitrile for dehydration. The dehydrated gel was incubated in 10 mM dithiothreitol and 100 mM NH_4HCO_3 at 56°C for 1 h. To prevent the digestion of Cys residues at the C termini by endoproteinase Asp-N, alkylation of the gels was carried out in 55 mM iodoacetamide and 100 mM NH_4HCO_3 at 25°C for 45 min in the dark. Finally, gel pieces were washed twice with 100 mM ammonium carbonate dissolved in acetonitrile and were dried completely before digestion. An immersed volume of endoproteinase Asp-N solution (10 μg/ml Asp-N and 50 mM NH_4HCO_3) was added to the dried gel and incubated at 37°C overnight, and the supernatant (the digested solution) after centrifugation was transferred to a new centrifuge tube. The precipitated gels were washed first with 20 μl of 20 mM NH_4HCO_3 and then with 20 μl of 50% (vol/vol) acetonitrile in 5% (vol/vol) formic acid, and the washed solutions were mixed with the digested solution and dried completely under a vacuum. The digested mixtures were applied to a ZipTip C_{18} column (Millipore, Tokyo, Japan). After a wash with 0.1% (vol/vol) trifluoroacetic acid, the peptides were eluted with 1 μl of 0.1% (vol/vol) trifluoroacetic acid dissolved in 75% (vol/vol) acetonitrile. Samples with 10 mg of 2,5-dihydroxybenzoic acid per ml of 33% acetonitrile matrix were analyzed by matrix-assisted laser desorption ionization–time-of-flight mass spectrometry (MALDI-TOF MS) using a MALDI-quadrupole-TOF tandem MS (MS-MS) QStar Pulsar *i* system (Applied Biosystems, Foster City, CA) in the linear positive-ion mode following the method of Hitachi Science Systems (Ibaraki, Japan).

Flotation assay. The flotation assay was carried out according to the method of Lecat et al. (14). Briefly, 10 million transfected or infected cells were washed with ice-cold PBS and then harvested with a rubber policeman. Collected cells were suspended in 0.6 ml of TNE buffer (25 mM Tris-HCl [pH 7.4] containing 150 mM NaCl, a protease inhibitor mix [Nacalai Tesque], and 5 mM EDTA) and then homogenated with a Dounce homogenizer or suspended with a 24-gauge needle. Each homogenate was incubated for 30 min on ice with or without 1% Triton X-100. The lysates were mixed with 0.4 ml of Optiprep (Sigma) to a final concentration of 40%. This mixture was overlaid with 1.2 ml of 30%, 1.2 ml of 25%, and 0.8 ml of 5% Optiprep and was then centrifuged at 42,000 rpm and 4°C for 5 h in an SW50 rotor (Beckman Coulter, Fullerton, CA). Each fraction was collected as 0.4 ml from the top of the centrifuging tube and was then precipitated with 4 volumes of cold acetone. The pellets were resolved in the loading buffer, boiled, and then subjected to SDS-PAGE and Western blotting. The fractions containing calreticulin, which is resident in the ER, in the absence and presence of the detergent were defined as the membrane and detergent-soluble fractions, respectively. In the presence of the detergent, the fractions with caveolin-1 were defined as the detergent-resistant fractions.

Quantitative real-time PCR. Total RNA was prepared from Huh7OK1 cells persistently infected with the JFH-1 virus or 9-13 cells by using an RNeasy minikit (Qiagen, Tokyo, Japan). The HCV genomic RNA was reverse transcribed and amplified by using a TaqMan EZ RT-PCR reagent kit (Applied Biosystems) with sense (5′-GAG TGT CGT GCA GCC TCC A-3′) and antisense (5′-CAC TCG CAA GCA CCC TAT CA-3′) primers corresponding to nucleotides 98 to 116 and 294 to 313, respectively. The kinetics of cDNA amplification were monitored by an ABI Prism 7000 sequence detection system (Applied Biosystems) using a reporter probe corresponding to nucleotides 238 to 267 of the 5′-conserved region for the HCV genotypes (5′-GCC CGC AAG ACT GCT AGC CGA GTA GTG TTG G-3′) conjugated with 6-carboxyfluorescein and 6-carboxytetramethylrhodamine at the 5′ and 3′ termini, respectively. A serial dilution of the partial HCV RNA synthesized by in vitro transcription from plasmids encoding the 5′-terminal region of HCV cDNA under the control of a T7 promoter was used as the standard for HCV genomic RNA. Intracellular GAPDH mRNA was also amplified using the TaqMan Pre-Developed Assay Reagent human GAPDH (Applied Biosystems). The values for HCV genomic RNA were normalized to those for GAPDH mRNA.

Quantitative detection of HCV core protein by ELISA. HCV core protein was quantified by using an Ortho HCV antigen enzyme-linked immunosorbent assay (ELISA) (Ortho Clinical Diagnostics, Tokyo, Japan) according to the manufacturer's instructions. Huh7.5.1 cells were transfected with pHH21/JFH-1/L758V or its mutants by lipofection. Cells and culture supernatants were harvested at 2, 4, 6, or 8 days after transfection. To determine the amounts of the intracellular core protein, cells were lysed with Triton lysis buffer on ice and subjected to the ELISA after 100- to 10,000-fold dilutions with PBS. Total protein levels were determined with a Micro BCA protein assay reagent kit (Pierce). Amounts of intracellular and extracellular core protein were normalized to total-protein amounts.

Immunofluorescent assay. Transfected Huh7.5.1 cells were fixed with a cold acetone-and-methanol mixture (50:50, vol/vol). After being blocked with 1% normal goat serum, cells were incubated with a mouse monoclonal antibody to NS5A at 4°C for 16 h, washed three times with PBS containing 0.5% Tween 20, and then incubated with an Alexa Fluor 594-conjugated antibody to mouse immunoglobulin G (Invitrogen). Cell nuclei were stained with Hoechst dye. The stained cells were washed three times with PBS containing 0.5% Tween 20 and then observed with a FluoView FV1000 laser scanning confocal microscope (Olympus, Tokyo, Japan).

RESULTS

Mutation in the HCV core protein confers resistance to SPP cleavage. Amino acid residues Ala^{180}, Ser^{183}, and Cys^{184} of the HCV core protein have been shown by others to be essential for intramembrane processing by SPP (10, 21), although our data suggested that Ile^{176} and Phe^{177}, but not Ala^{180}, Ser^{183}, and Cys^{184}, were required for the processing of the HCV core protein by SPP (30). To clarify this discrepancy, we constructed an N-terminally FLAG-tagged and C-terminally HA-tagged wild-type HCV core protein and similarly tagged mutant core proteins in which Ala^{180}, Ser^{183}, and Cys^{184} were replaced with Val, Leu, and Val, respectively (referred to below as Core ASC/VLV, or M1) (21), or Ile^{176} and Phe^{177} were replaced with Ala and Leu, respectively (referred to below as Core IF/AL, or M2) (30). We then expressed these core proteins in 293T cells (Fig. 1). Ala^{191} was replaced with Arg in these FLAG-core-HA constructs to prevent cleavage by SP (7), and only the SPP-resistant core protein was detected by an anti-HA

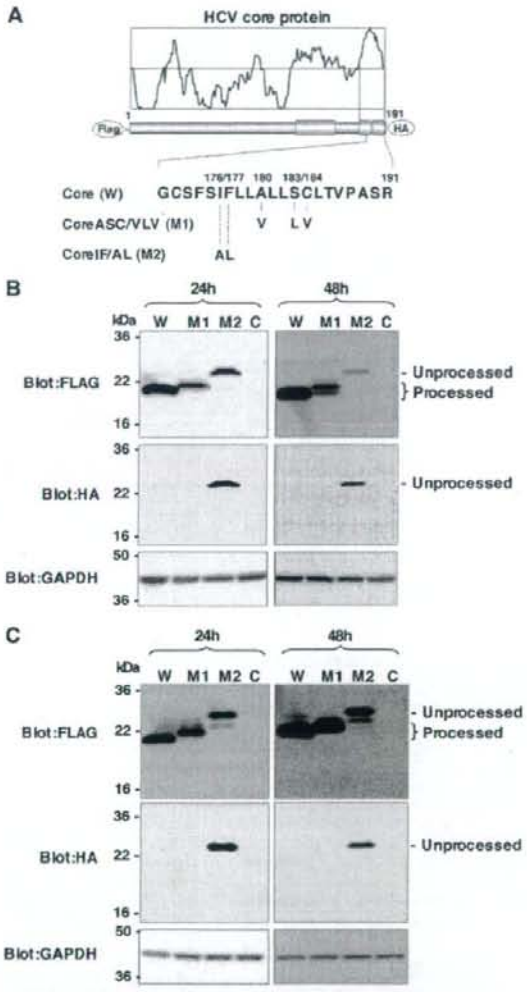

FIG. 1. Effects of mutations in the HCV core protein on cleavage by SPP. (A) cDNA constructs encoding the N-terminally FLAG- and C-terminally HA-tagged wild-type HCV core protein (W), Core ASC/VLV (M1), and Core IF/AL (M2). The Ala at amino acid residue 191 of all constructs was mutated to Arg in order to prevent the processing of an HA tag by SP. (B) Each of the core constructs or an empty vector (lane C) was transfected into 293T cells. Cell lysates harvested at 24 or 48 h posttransfection were subjected to Western blotting using antibodies against the indicated proteins. (C) Cells transfected with each of the core constructs or an empty vector were treated with 15 μM MG132 for 5 h and examined as described for panel B.

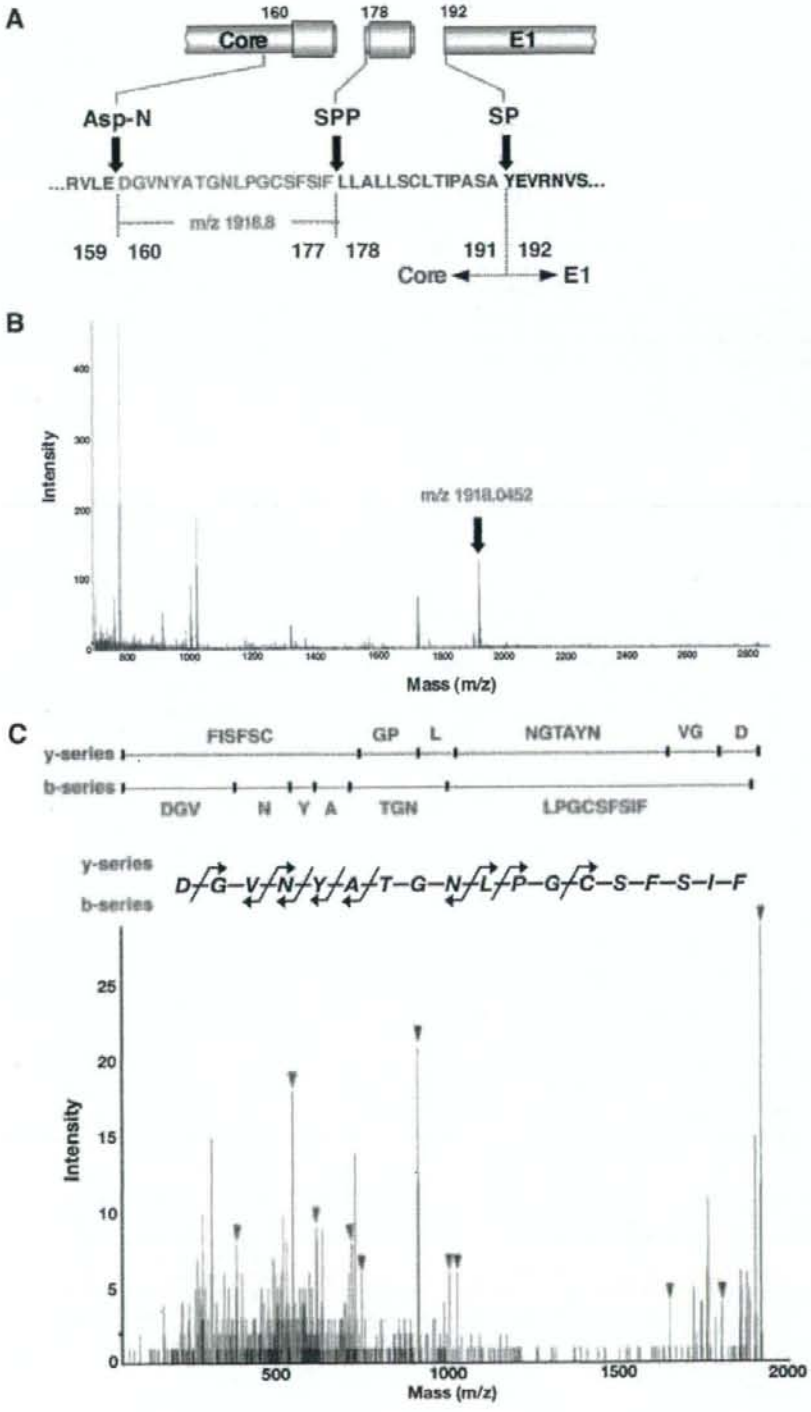

antibody in this experimental setting. Core IF/AL was detected in cells by both anti-FLAG and anti-HA antibodies at 24 h and 48 h posttransfection, whereas the wild-type core and Core ASC/VLV were detected by an anti-FLAG antibody but not by an anti-HA antibody (Fig. 1B). These results indicate that Core IF/AL is resistant to SPP cleavage, in contrast to the complete processing of the wild-type core and Core ASC/VLV. Although Core ASC/VLV exhibited a single band that was slightly larger than the wild-type core protein at 24 h posttransfection, an extra band with the same mobility as the wild-type core protein appeared at 48 h posttransfection (Fig. 1B), suggesting that the introduction of mutations in Ala^{180}, Ser^{183}, and Cys^{184} induces multiple processing in the signal sequence of the mutant core protein. To exclude the possibility that unprocessed Core ASC/VLV is degraded by a proteasome due to misfolding, each of the core constructs or the empty vector was transfected into 293T cells and treated with a proteasome inhibitor for 5 h. The unprocessed band of Core IF/AL, but not that of Core ASC/VLV, was detected by the anti-HA antibody (Fig. 1C). These results further support the notion that Core ASC/VLV is sensitive to SPP-dependent processing. Bands observed between unprocessed and processed proteins in cells expressing wild-type core or Core IF/AL in the presence of a proteasome inhibitor were not detected by the anti-HA antibody, suggesting that these products are generated by C-terminal truncation and are sensitive to proteasome degradation.

Identification of the C-terminal residue of the mature HCV core protein. Previous reports have suggested that the C terminus of the mature HCV core protein expressed in insect cells by using a baculovirus expression system is Phe^{177} (29) or Leu^{179} (12). To clarify the C-terminal amino acid residue of the mature HCV core protein expressed in human cells, a purified fragment of the HCV core protein was analyzed by MALDI-TOF MS. The FLAG-tagged HCV core protein was expressed under the control of a CAG promoter in 293T cells, purified by immunoprecipitation with beads conjugated with the anti-FLAG antibody, and then released from the beads by the addition of free FLAG peptide. The purified FLAG-tagged core protein was digested with Asp-N protease, and the final sample was subjected to MALDI-TOF MS for determination of the C-terminal residue. The N-terminal amino acid of the peptide fragment including the C terminus of the mature HCV core protein was expected to be Asp^{160} (Fig. 2A). The peptide fragment with an *m/z* of 1,918.0452, which is close to the calculated value (*m/z* 1,918.8) of the sequence DGVNYATG NLPGCSFSIF (Fig. 2A), was detected, and no larger peak was evident (Fig. 2B). MS-MS analysis showed that the fragment has the amino acid sequence DGVNYATGNLPGCSFSIF (Fig. 2C). These results indicate that the C terminus of the mature HCV core protein expressed in human cells is Phe^{177}. This is consistent with our previous observation (30) and with the data shown in Fig. 1, which indicate that the M2 mutation completely abrogated the processing of core protein by SPP. Both Ile^{176} and Phe^{177} may play crucial roles in recognition by SPP for intramembrane cleaving activity.

SPP processing is required for the localization of HCV core protein in the DRM. Based on confocal microscopy observations, Matto et al. reported that the HCV core protein associates with a DRM that is distinct from the classical raft fraction, as evidenced by the lack of colocalization of typical raft markers, including caveolin-1 and the B subunit of the cholera toxin, which binds to glycosphingolipid GM1 in the plasma membrane (20). We have previously suggested that intramembrane processing by SPP affects the intracellular localization of the HCV core protein, and the replacement of Leu^{139}, Val^{140}, and Leu^{144} with Ala in the HCV core protein (Core LVL/3A [M3]) (Fig. 3A) abrogated SPP-mediated processing and ER retention (30). In this study, we examined the effect of SPP cleavage on the DRM localization of the HCV core protein. The wild-type or mutant HCV core protein was expressed in 293T cells, solubilized at 4°C in the presence or absence of 1% Triton X-100, and subjected to sucrose gradient centrifugation. Fractions were collected after ultracentrifugation and analyzed by immunoblotting. The wild-type core protein was partially detected in fraction 3, which corresponded to the DRM fraction, and was mainly detected in the detergent-soluble fraction (Fig. 3B). However, the mutant core proteins Core LVL/3A (M3) and Core IF/AL (M2) were localized in the membrane fraction but not in the DRM fraction (Fig. 3B). Although the M2 mutant exhibits clear resistance to SPP-dependent cleavage, as shown in Fig. 1B, processed core proteins of M2 and M3 mutants were detected by flotation analyses (Fig. 3B), suggesting that the M2 and M3 mutants are cleaved by unknown mechanisms during the concentration step. These results suggest that processing by SPP is required for the DRM localization of the HCV core protein.

A dominant-negative SPP mutant inhibits the intramembrane processing and DRM localization of the HCV core protein. SPP belongs to the family of aspartic proteases, which share two Asp residues for the active sites of protease activity. Asp^{219} and Asp^{264} have been identified as active sites for the protease activity of SPP (48). Overexpression of the SPP mutant in which Asp^{219} was replaced with Ala (SPPD219A) resulted in a dominant-negative activity that prevented the intramembrane processing of the HCV core protein (30). To examine the relationship between intramembrane processing by SPP and the localization of the HCV core protein in the DRM fraction, a C-terminally HA-tagged wild-type (SPP-HA)

FIG. 2. Determination of the C termini of the mature HCV core protein. (A) Schematic representation of the junction between the core and E1 proteins. The cleavage sites for the exogenous Asp-N protease and the host SP were the N-terminal residue Asp^{160} and the C-terminal residue Ala^{191}, respectively. The cleavage site of the host SPP was determined to be the C-terminal residue Phe^{177} in this study. The expected *m/z* of the peptide fragment (spanning residues 160 to 177) processed by the Asp-N protease and SPP is indicated. (B) The FLAG-core protein was purified with an anti-FLAG antibody, digested with Asp-N, and analyzed on a 2,5-dihydroxybenzoic acid matrix by MALDI-TOF MS in the linear positive-ion mode. The peak at *m/z* 1,918.0452 corresponded to the expected fragment (*m/z* 1,918.8) derived from the Asp-N- and SPP-digested core protein, DGVNYATGNLPGCSFSIF. (C) The peak at *m/z* 1,918.0452 was subjected to MS-MS analysis with a MALDI-Qq-TOF MS-MS QStar Pulsar *i* system. The resulting spectrum was applied to MASCOT to determine the amino acid sequence. The analyzed peak at *m/z* 1,918.0452 corresponded to the sequence DGVNYATGNLPGCSFSIF.